UNIVERSITY OF OKLAHOMA

GRADUATE COLLEGE

MICROSEISMIC LOCATION USING DIFFERENTIAL BACKAZIMUTH ANGLES

A THESIS

SUBMITTED TO THE GRADUATE FACULTY

in partial fulfillment of the requirements for the

Degree of

MASTER OF SCIENCE

By

RAE TRAVIS JACOBSEN
Norman, Oklahoma
2016

MICROSEISMIC LOCATION USING DIFFERENTIAL BACKAZIMUTH ANGLES

A THESIS APPROVED FOR THE
CONOCOPHILLIPS SCHOOL OF GEOLOGY AND GEOPHYSICS

BY

_____
Dr. Kurt Marfurt, Chair

_____
Dr. Jamie Rich

_____
Dr. John Pigott

Acknowledgements

I would like to thank Dr. Jamie Rich for taking me on as a graduate student and his patience for working with a geologist who arrived with very little geophysics experience. Dr. Kurt Marfurt and Dr. John Pigott have been hugely important to my success at The University of Oklahoma, and I am indebted to them for their participation on my committee. My fellow geophysics graduate students also had a great impact on the completion of my thesis work. They acted as sounding boards to help me through the pain of coding and other technical problems. I must give a special thanks to Abdulmohsen Alali, who has been selfless in his willingness to spend time helping me. Thank you to Jackson Haffener and Xuan Qi for providing coding ideas and help in MatLab. I also appreciate all the time and effort the geology and geophysics staff has provided to make my time as a graduate student go smoothly. Thank you to my friends and family who have given their support and helped me remain focused. Lastly, my deepest gratitude goes out to my wife Melissa, whose feedback, encouragement, and love kept me going during this two year adventure.

Table of Contents

Acknowledgements iv

List of Figures vii

Abstract xii

Chapter 1: Introduction 1

Chapter 2: Background Research 3

Geologic Background of the Granite Wash 3

Source Location Methods Background 4

Geiger's Method 4

Hodogram Analysis 5

Double-Difference Method 6

Optimization Background 9

Grid Search 9

Gradient Descent 9

Chapter 3: Methods 16

Grid Search 16

Optimization- Gradient Descent 18

Perf Shot Data Application 19

Chapter 4: Results 22

Grid Search 22

Gradient Descent 23

Perf Shot Data Application 24

Chapter 5: Discussion 35

Grid Search 35

Gradient Descent 37

Perf Shot Data Application 39

Chapter 6: Conclusions 47

References 49

List of Figures

Figure 1. Location of the study area within the Anadarko Basin near Allison, Texas (after Durrani et al., 2014).....11

Figure 2. Schematic of the Amarillo Uplift and its erosion into the Anadarko Basin forming the Granite Wash formation (Mitchell, 2011). 11

Figure 3. An earthquake seismogram with first arrivals labeled. Time difference in P and S waves formulate the objective function for the Geiger Method (after British Geological Survey, 2016).....12

Figure 4. (a) Schematic of the traditional, Geiger Method. Known geophone orientation provides direction to event, known velocity model provides distances from receiver to event. (b) Schematic cross section showing one event and a downhole array of 3 component geophones. 13

Figure 5. (a) Microseismic events located with a traditional approach in the horizontal plane. Due to close events sharing common ray paths (purple lines) the residuals from travel time differences can be utilized to relocate events. (b) Relocated events using the double difference. 14

Figure 6. Schematic of several search/optimization algorithms plotted in relation to their ability to search the parameter space (Exploration) and exploit information to reach the desired minimum/maximum (Exploitation). I will implement the uniform search (grid search) and gradient descent (Sambridge and Mosegaard, 2002). 15

Figure 7. Schematic hodogram of particle motion in the *x, y* plane; detected by a three component geophone (after Ge, 2003). 20

Figure 8. (a) Schematic of the back azimuth location method. Event are located without any velocity model information. (b) Schematic cross section showing two events used for the back azimuth analysis. 21
Figure 9. Contoured objective function (units in ft) where event 1 is fixed and its absolute location shown (red X). 25
Figure 10. Scatter plot of the absolute locations of the two events and the calculated guesses. See contour plot above. 25
Figure 11. Contoured objective function (units in ft) where event 1 is fixed and its absolute location shown (red X). Events are nearly 15 ft apart from one another, but both events are off from sampled nodes. 26
Figure 12. Scatter plot of the absolute locations of the two events and the calculated guesses. See contour plot above. 26
Figure 13. Contoured objective function (units in ft) where event 1 is fixed and its absolute location shown (red X). Events are nearly 700 ft apart from one another with only event one being located on a node. 27
Figure 14. Scatter plot of the absolute locations of the two events and the calculated guesses. See contour plot above. 27
Figure 15. Contoured objective function (units in ft) where event 1 is fixed and its absolute location shown (red X). Events are nearly 1500 ft apart from one another; both events are located on nodes. 28
Figure 16. Scatter plot of the absolute locations of the two events and the calculated guesses. See contour plot above. 28

Figure 17. Contoured objective function (units in ft) where event 1 is fixed and its absolute location shown (red X). Events are nearly 15 ft apart from one another and located on nodes near the grid boundary. 29

Figure 18. Scatter plot of the absolute locations of the two events and the calculated guesses. See contour plot above. 29

Figure 19. Contoured objective function (units in ft) where event 1 is fixed and its absolute location shown (red X). Absolute location of event one is on a node while the second event's absolute location is off the grid. 30

Figure 20. Scatter plot of the absolute locations of the two events and the calculated guesses. See contour plot above. 30

Figure 21. Gradient descent models reveal that microseismic source location can be determined using only azimuth information. Red x's are the known locations, green +'s are the calculated locations, purple Δ's are initial guess solutions, and blue o's are monitor wells. 31

Figure 22. Cost function for gradient descent location shown in Figure 21. Algorithm convergence is generally obtained within 2000 iterations. 32

Figure 23. Gradient descent search algorithm applied to a realistic monitor array geometry. Inset map displays monitor array geometry with the *x, y* axes having the same scale. When the algorithm's initial guess is close to the absolute location the differential backazimuth method provides accurate locations. Red x's are the known locations, green +'s are the calculated locations, purple Δ's are initial guess solutions, and blue o's are monitor wells. 33

Figure 24. Cost function of the gradient descent applied to a realistic monitor well array geometry (see Figure 23). Real array geometry requires an initial guess that has a small objective function. Plot is magnified to verify function's convergence. 34
Figure 25. Schematic of the sampling of grid search in order to find the minimum of the contoured objective function. The sampling error of grid search may be under sampling the objective function and causing error in the calculated locations. 41
Figure 26. The contoured velocity model anomalies taken from velocity information at the three monitor wells. Brown star indicates a microseismic event located outside the array using the wells' velocity model. 42
Figure 27. The actual velocity model anomalies for the area. The velocity model in Figure 26 would not image the northern anomaly and using the velocity model for the northern event (red star) would result in high location error. 42
Figure 28. Schematic of the reported well path and the actual well path. Calibration shot locations based on reported well paths often have location errors that will affect geophones when an orientation correction is applied. 43
Figure 29. Modified location workflow that incorporates the differential backazimuth method in either the first or second step for a calibrated velocity model. 44
Figure 30. Schematic of two stages of microseismic events that have been located using the traditional approach with a poor velocity model. Notice the wide spacing of events in microseismic clouds. 45
Figure 31. Schematic of two stages of microseismic events that have been located using the modified location approach that incorporates the backazimuth method. The backazimuth method would allow for better calibration of the velocity model.

Microseismic clouds would collapse to better image fractures resulting from hydraulic stimulation. 46

Abstract

The most common procedure for locating borehole microseismic events is solution of a minimization problem based on observed travel time differences compared to calculated travel time differences derived from a given velocity model and oriented geophones. However, both the velocity model and geophone corrections often contain errors that will incorrectly locate microseismic events. An alternate method characterizes events using only their differential backazimuth information, based only on the difference in backazimuth angles between multiple microseismic events observed at common monitor wells. Possible locations are then found by using the grid search and gradient descent search algorithm finding the minimum residual between measured and calculated differential backazimuth angles.

Microseismic events can be located in the horizontal plane with only differential backazimuth information. The gradient descent search is significantly faster than exhaustive search and can be applied to real array geometries. Tests from the array geometry near Allison, Texas targeting the Granite Wash Formation indicate this method can locate events even when array geometry is very poor. Owing to the non-ideal array geometry, required initial guesses must be within 50 ft to ensure convergence to the global minimum. The backazimuth method can be implemented to locate microseismic events where the velocity model is poor. By first locating events using the backazimuth approach, the velocity model can be constrained and calibrated for subsequent locations.

Chapter 1: Introduction

Microseismic imaging of hydraulic fractures relies on the detection of microearthquakes associated with either fracture creation or induced movement of preexisting fractures (Maxwell, 2002). Detected events are utilized to understand the extent of hydraulic fractures and the amount of rock volume stimulated. Bore hole microseismic event location depends on a carefully calibrated velocity model and accurate orientation of geophones. When these criteria are met, traditional location methods such as Geiger's (1912) Method can be employed to locate events. However, in some instances the area's velocity model can be poor due to anomalies and unmodeled velocity structures, which will lead to inaccurate event locations (Zimmer, 2011). Errors in geophone orientation will lead to mistakes in the azimuthal information used to place microseismic events. Waldhauser and Ellsworth (2000) improved the relative location of seismic events when a calibrated velocity model is unavailable by creating a method known as the Double Difference. Li et al. (2013) modified and applied the Double-Difference to microseismic events. However, location errors can persist even with these adjustments, demonstrating the need for an alternate location method independent of the velocity model and geophone orientation.

To develop the differential backazimuth location technique, I implemented exhaustive grid search and gradient descent as search algorithms to probe the parameter space. Results from grid search are accurate but can require high computation time; gradient descent has significantly less computation time and locates more events in a larger area. When real array geometries are applied to the gradient descent search,

events are accurately located in the horizontal plane. My workflow, implementing the differential backazimuth technique, can be used to calibrate the velocity model and provide accurate microseismic event locations.

Chapter 2: Background Research

Geologic Background of the Granite Wash

The Granite Wash is located across the North Texas Panhandle and western Oklahoma within the Anadarko Basin (Figure 1). The play extends 130 miles over 7 counties, encompassing nearly 2.5 million acres (LoCricchio, 2012). In the deepest part of the Anadarko Basin the Granite Wash can reach a total thickness of 1500 m and can thin to approximately 100 m (Long, 2014). Subunits within the Granite Wash range in age from the early Pennsylvanian (Morrow) to the early Permian (Chase/Council Grove). Many of these subunits contain hydrocarbons constituting stacked pay zones that are often separated by marine shales or carbonate layers.

The Amarillo and Wichita uplift created the Granite Wash Formation during the Late Mississippian-Early Pennsylvanian from intense northeast-southwest regional compression (Gay, 2014). During the uplift basement rock was exposed and eroded, resulting in many granite cobbles and clasts within the fan system and giving rise to the label "Granite Wash" (Figure 2). Most of these sediments were deposited in an alluvial fan environment where the sorting and clast size are directly related to proximity of the source. Porosity and permeability throughout the Granite Wash is low due to a high level of carbonate cement (Mitchell, 2011). Diagenesis has also influenced the low porosity and permeability in many reservoirs with minerals such as calcite, kaolinite, feldspars, quartz, and chlorite.

Source Location Methods Background

Geiger's Method

Geiger's method is the classic approach to locating seismic and microseismic events and was developed near the turn of the 20th century (Geiger, 1912). The method applies the Gauss Newton nonlinear optimization approach to evaluate the origin time and location of a seismic event by iterative linearization steps (Lee and Dodge, 2010). Earthquake seismology uses the method for local earthquake locations, but the technique can be applied to microseismic data to provide locations relative to a fixed coordinate system (absolute locations). For Geiger's method to work, one picks a set of arrival times from a station's seismogram (Figure 3) and estimates a velocity model for the area (Ge, 2003). Residuals between the observed travel time and calculated travel time are evaluated, where the calculated times are derived from the algorithm guessing possible source locations (Figure 4). Mathematically, the residual equation is

$$dr_k^i = (t_k^i)^{obs} - (t_k^i)^{cal} \quad (1)$$

where dr_k^i is the residual between observed and calculated arrival times, k is the geophone index, i is the event, and t is travel time arrivals. The partial derivative of the event location parameters creates an adjustment vector (Geiger, 1912), and the adjustment vector updates the initial guess after each iteration. Once the residual between measured and calculated arrival times falls below a pre-defined threshold the process terminates and the final calculated origin time and hypocenter parameters are deemed the solution.

Use of Geiger's Method is best when arrival times have high signal-to-noise ratios and a velocity model that accurately models the observed arrival times. High

signal-to-noise events allow for clear picks to be made with less error in arrival time picks than noisier data. Geophones must be widely distributed and the absolute orientation of each geophone must be known in order to correctly locate an event (Lee and Dodge, 2010). Areas with high geologic heterogeneities will result in complex velocity models where differences in the observed and calculated arrival times will be highly irregular. When these differences, or residuals, are plotted the image will appear multimodal, non-smooth, or discontinuous (Sambridge and Mosegaard, 2002). Thus the plot, or objective function, is considered to be complex and difficult to solve using linearization.

Stability of an objective function is an issue for every iterative method. When objective functions are complicated, convergence may take large amounts of time or simply not be reached. One must note that this method's location accuracy is highly dependent on the accuracy of the velocity model. Overall, the Geiger Method is an excellent first step to determining the absolute locations of microseismic events.

Hodogram Analysis

When multiple monitor wells are unavailable, a single monitor well can locate microseismic events though hodogram analysis. Hodogram analysis first requires a proper knowledge of the monitoring geometry (Maxwell, 2014). Well head position and borehole deviation surveys for the monitor well must be accurately measured with the correct reference system. Borehole array orientation is often difficult since the three-component geophones are randomly oriented when lowered into the borehole. Geophone orientations can be computed by recording a perforation shot or check shot from a known location. As seismic waves from these known sources arrive at the

monitor well, the P-wave pulse is identified. Owing to the particle motion of a P-wave being parallel to the direction of wave propagation, P-waves provide information useful in estimating the backazimuth to an event. Three component geophones record the P-wave's amplitude over time, and these recordings are cross-plotted as hodograms. The relative bearing of the *x*, *y* components are then computed to align the hodogram direction with the ray path direction of the known source (Maxwell, 2014). Multiple calibration shots from different locations are preferred to verify the accuracy and consistency of the analysis.

Microseismic interpreters use the oriented geophones, picked arrival times, and a calibrated velocity model to locate events within the area. However, locations are often biased towards events that are closer to the borehole array. This bias is due to closer events having higher SNR in comparison to events further away from the borehole array. For single monitor wells, hodogram analysis is necessary twice, once to orient the geophones and again to find the orientation of the event. Both iterations will have error associated with them. Input error can enter the analysis when the calibration events used for absolute orientation are mislocated, well paths are deviated, or arrivals are noisy.

Double-Difference Method

Waldhauser and Ellsworth in 2000 created the Double-Difference method as a way to relocate seismic events that had previously been located with techniques such as the Geiger Method. The Double-Difference exploits the residual between observed and calculated arrival times from multiple events and can greatly improve the relative location of events. Relative location is an event's location relative to others in the

vicinity; these relative locations are affected less by the velocity model in comparison to absolute locations (Slunga et al., 1995). The technique is most effective in regions with a dense distribution of events where the distance between neighboring events is small compared to the source-receiver distances (Waldhauser and Ellsworth, 2000). Improvements in relative location are due to events close to one another sharing the same ray path, thus changes in the velocity model do not affect their relative locations. The Double-Difference method exploits this information by subtracting the calculated arrival time residuals from the observed arrival time residuals, which is expressed mathematically as

$$dr_k^{ij} = (t_k^i - t_k^j)^{obs} - (t_k^i - t_k^j)^{cal} \quad (2)$$

Where dr_k^{ij} is the residual between observed and calculated differential arrival times, k is the geophone index, i, j are events, and t is travel time arrivals.

Major improvements in the relative location of seismic events generally result from applying the Double-Difference technique (Figure 5). Events that once appeared in large spatial distributions tend to collapse to image very fine structures along fault zones (Waldhauser and Ellsworth, 2000). The technique is intended to reduce the effect of errors from velocity heterogeneities not accounted for in the velocity model. These errors will heavily affect the absolute locations, but the relative locations derived from the Double-Difference will generally remain unaffected. In general, the Double-Difference technique is useful in relocating seismic events to obtain a more accurate relative location, and is most effective in regions with a dense distribution of seismicity where the distance between neighboring events is small.

Slight changes have been applied to the Double-Difference in an effort to build upon Waldhauser and Ellsworth's findings and transition the method from seismic to microseismic events. Application of the Double-Difference technique to microseismic events has resulted in better relative locations. Li et al., (2013) attempted to minimize input error by exploiting differential backazimuths in a modified Double-Difference location algorithm. They express the residual between observed and calculated arrival times as

$$r_k^i = (t_k^i)^{obs} - (t_k^i)^{cal} = \sum_{l=1}^{3} \frac{\partial T_k^i}{\partial x_l^i} \Delta x_l^i + \Delta \tau^i, \tag{3}$$

and follow with the Double-Difference applied to microseismic events expressed as

$$r_k^i - r_k^j = \sum_{l=1}^{3} \frac{\partial T_k^i}{\partial x_l^i} \Delta x_l^i + \Delta \tau^i - \sum_{l=1}^{3} \frac{\partial T_k^j}{\partial x_l^j} \Delta x_l^j + \Delta \tau^j. \tag{4}$$

They then show the double difference can be extended to backazimuths from the two events (i, j) to a single monitor well (k) as

$$\varphi r_k^i - \varphi r_k^i = \sum_{l=1}^{3} \frac{\partial \varphi_k^i}{\partial x_l^i} \Delta x_l^i - \sum_{l=1}^{3} \frac{\partial \varphi_k^j}{\partial x_l^j} \Delta x_l^j. \tag{5}$$

By running a simultaneous double difference of arrival times and backazimuths Li et al., 2013 show that the method could provide better relative locations for events, which would define fractures and fault zones with higher accuracy. As with the original Double-Difference technique, this modification performs best in regions with a dense distribution of seismicity where neighboring events can be easily linked.

Optimization Background

Grid Search

Grid search is a simple deterministic approach of dividing a parameter space into a uniform array of cells and analyzing each cell against a given criteria (Sambridge and Mosegaard, 2002). When the search area is small and the number of unknowns is few, this method can be an effective forward model to solve for event locations. Due to the even distribution of grid cells, the search is unbiased and can be very accurate.

This method grew into popularity during the 1950's due to the increased advances in computer technology and processing. In the early 2000's seismologists began applying grid search to locate seismic events (Lee and Dodge, 2010). Overall, grid search is a useful way to test event location algorithms and understand the optimization convergence criterion necessary for event location.

Gradient Descent

Gradient descent is an optimization approach where the objective function's first derivative is used to find its minimum. For each iteration of the algorithm, the gradient is recalculated such that the current estimate continues to move towards the minimum value, which for location methods corresponds to the calculated location of a microseismic event. Gradient descent exploits the gradient in order to minimize the objective function, but it lacks the ability to thoroughly search the parameter space (Figure 6). Thus, the technique relies on choosing an initial guess, or trial solution, for the first iteration close to the global minimum. Picking an initial guess far away from the actual minimum may cause computation time to increase, or worse result in a local minimum solution. This classical method has been used extensively to solve nonlinear

equations (Ge, 2003). Valleys or saddle points in the objective function can give rise to numerical instabilities. These features are often caused by poorly conditioned objective functions or matrices (Sambridge and Mosegaard, 2002).

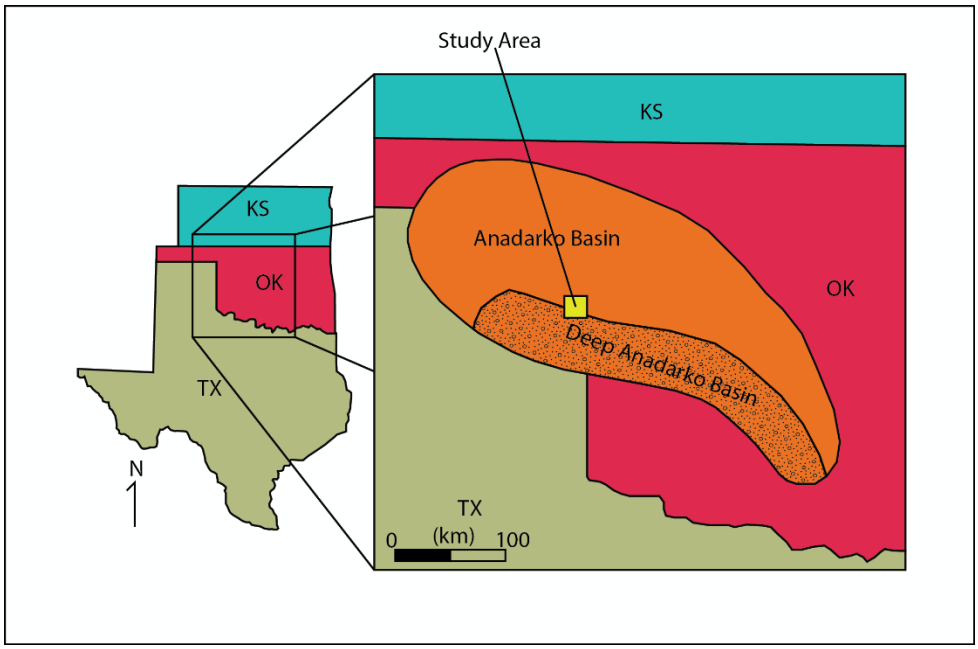

Figure 1. Location of the study area within the Anadarko Basin near Allison, Texas (after Durrani et al., 2014).

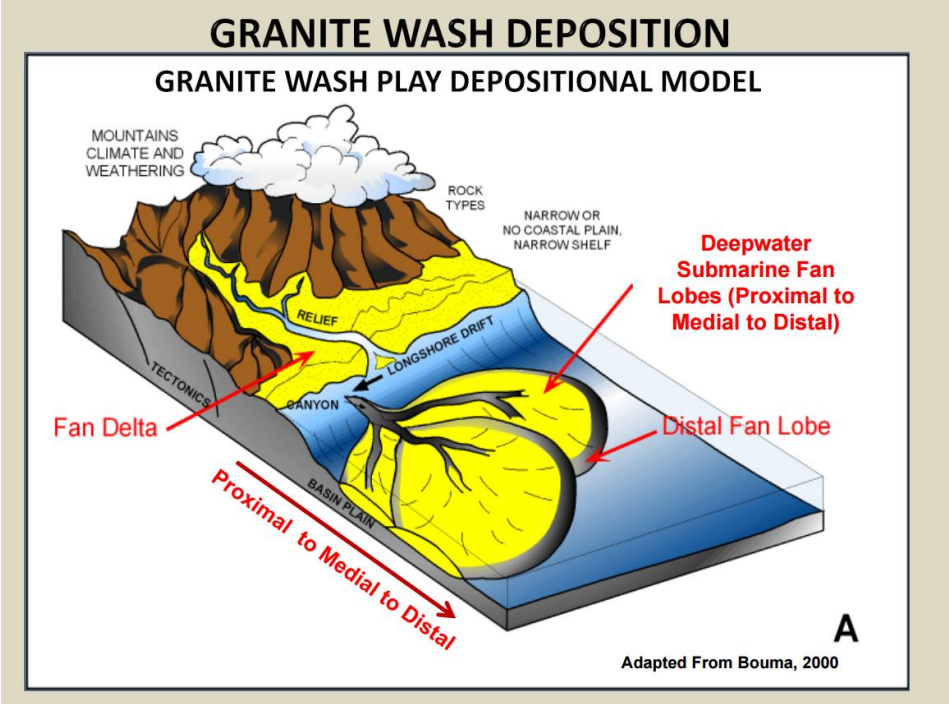

Figure 2. Schematic of the Amarillo Uplift and its erosion into the Anadarko Basin forming the Granite Wash formation (Mitchell, 2011).

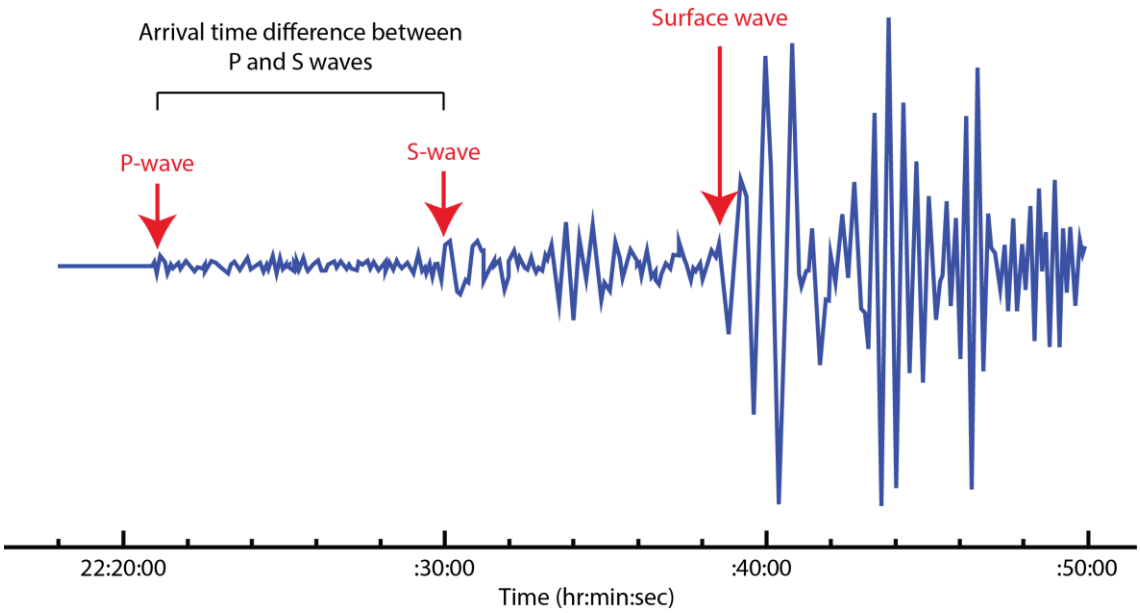

Figure 3. An earthquake seismogram with first arrivals labeled. Time difference in P and S waves formulate the objective function for the Geiger Method (after British Geological Survey, 2016).

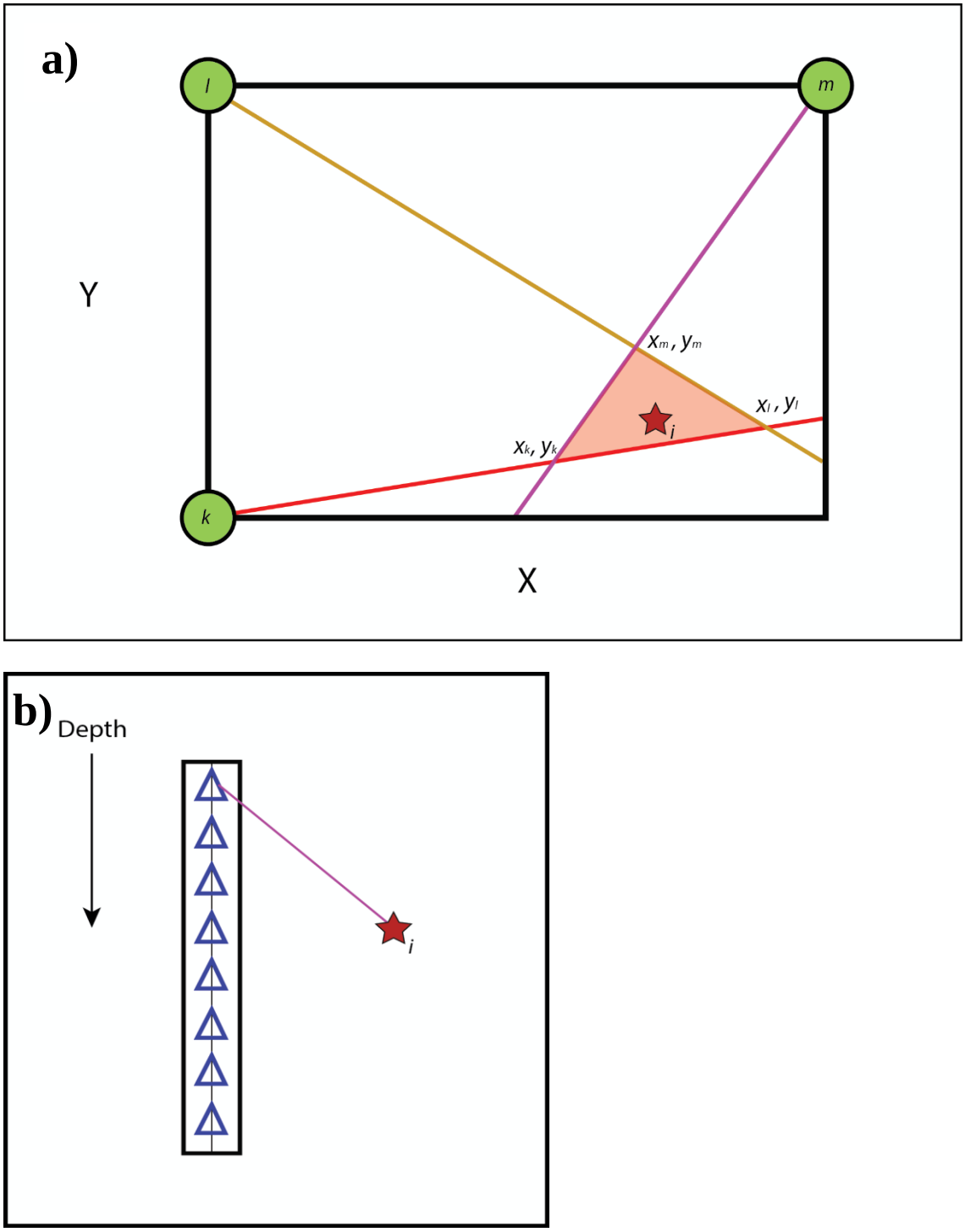

Figure 4. (a) Schematic of the traditional, Geiger Method. Known geophone orientation provides direction to event, known velocity model provides distances from receiver to event. (b) Schematic cross section showing one event and a downhole array of 3 component geophones.

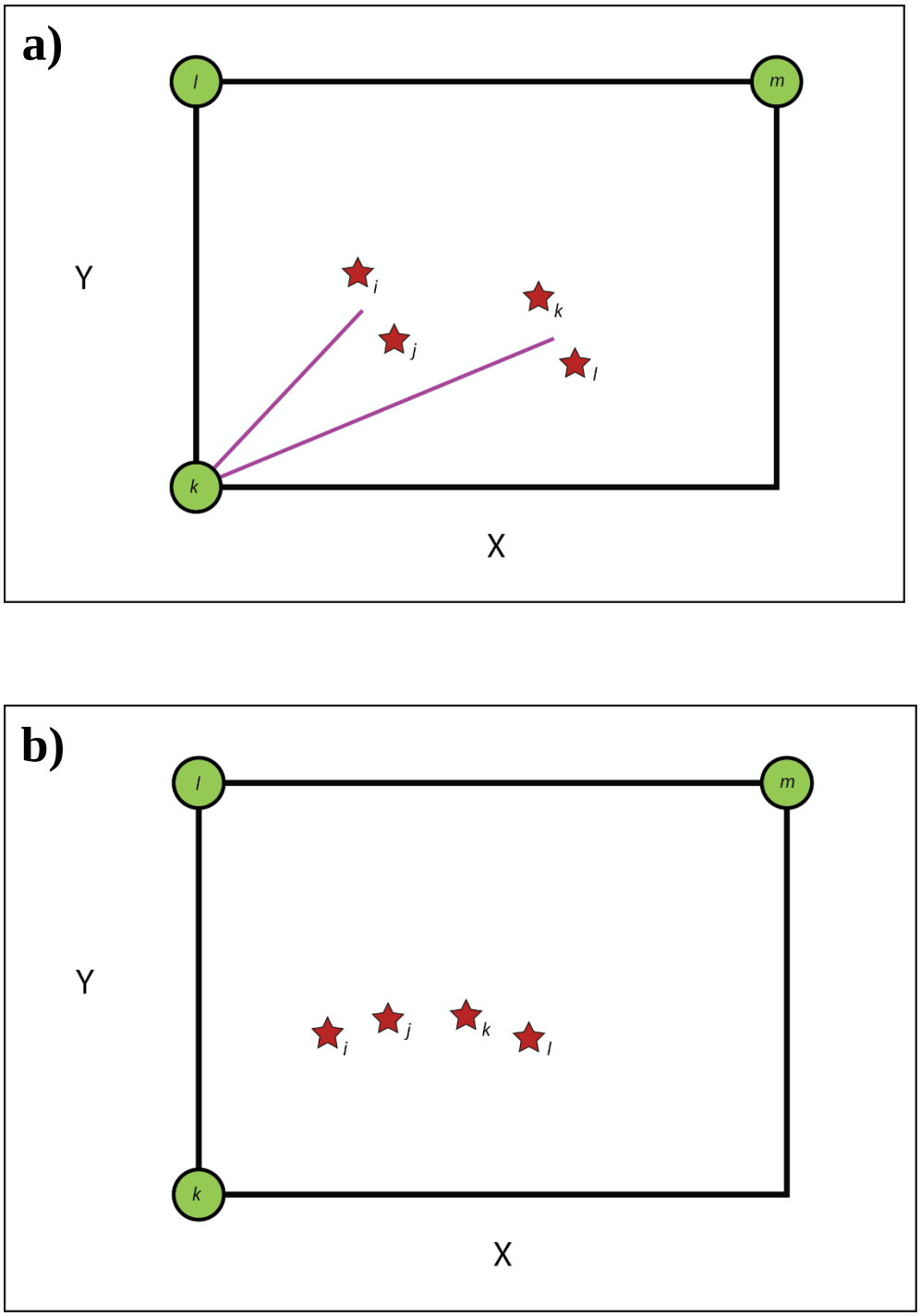

Figure 5. (a) Microseismic events located with a traditional approach in the horizontal plane. Due to close events sharing common ray paths (purple lines) the residuals from travel time differences can be utilized to relocate events. (b) Relocated events using the double difference.

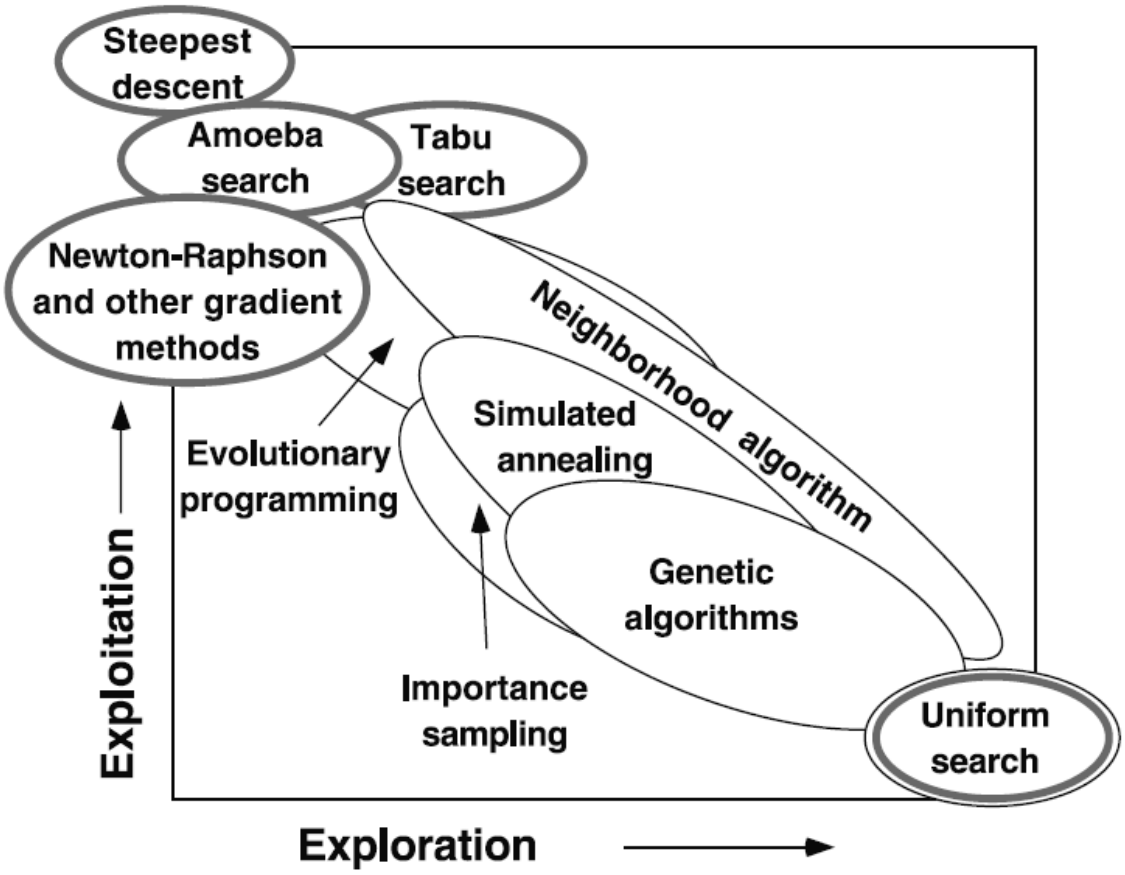

Figure 6. Schematic of several search/optimization algorithms plotted in relation to their ability to search the parameter space (Exploration) and exploit information to reach the desired minimum/maximum (Exploitation). I will implement the uniform search (grid search) and gradient descent (Sambridge and Mosegaard, 2002).

Chapter 3: Methods

In order to locate microseismic events using only differential backazimuth information, I tested the objective function and determined a possible optimization technique, simultaneously located two or more events, and applied the method to a realistic, non-ideal monitor array geometry. By implementing grid search to the objective function multiple events were simultaneously located with gradient descent optimization, and applied real monitor array geometry by using perforation shot data acquired near Allison, Texas. These methods are explained in detail below.

Grid Search

By using a grid search method I was able to test the proposed objective function and discover its capabilities and limits. The objective function's structure was drawn from the information acquired from hodograms. The backazimuth can be determined by the relative amplitude of the two orthogonal horizontal components of either the P or S wave arrivals. For my synthetic grid search models, the absolute location of the events are known. Owing to this, the observed back azimuth angle that normally is derived from hodograms has been replaced by the angle between the known sources and the monitor wells (Figure 7).

Location of events as shown in Figure 8 relies on finding the *x, y* position of the two events simultaneously such that the measured differential azimuth angle from hodogram analysis match the calculated differential azimuth angle. The simplest case for two events can be implemented using a grid search where the numeric function to be minimized is

$$f(x_1, y_1, x_2, y_2) = \sqrt{\sum_{i=1}^{3} \text{ATAN2}[\sin(\Delta\theta_i^m - \Delta\theta_i^c), \cos(\Delta\theta_i^m - \Delta\theta_i^c)]^2} \quad , \tag{6}$$

and

$$\Delta\theta_i^c = \text{ATAN2}(\sin(\text{ATAN2}(y_1 - y_i^w, x_1 - x_i^w)), \cos(\text{ATAN2}(y_2 - y_i^w, x_2 - x_i^w))). \tag{7}$$

Grid search evaluates all possible values of x_i and y_i with the value that minimizes the function deemed the solution. This is satisfactory for small grids and only two events, but a generalization is necessary when simultaneously considering more than two events.

The model is designed with dimensions of 1500 X 1500 ft, which was divided into an array of 100 X 100 cells; three monitor wells are placed at the edges of the grid and two events are located using the objective function described earlier. Known well locations and the true azimuths to the events are input into the program. The program searches through every sampling point (nodes) on the grid to calculate azimuths and assign an error value, where the error is the residual between $\Delta\theta_i^m$ and $\Delta\theta_i^c$ (Equation 6). After all cell locations have been evaluated, the location with the lowest residual is determined and the events are assigned to that corresponding location. Computation time to run this search rises geometrically as the grid area is expanded, which further reinforced the need to adapt the algorithm to run in an optimization approach.

Optimization- Gradient Descent

In the case of more than two events I implement a gradient decent algorithm. The number of unique combination of possible event locations becomes $(N_x * N_y)^{N_e}$ where N_e is the number of events, N_x is the number of *x* grid cells, and N_y is the number of *y* grid cells; my initial case used two microseismic events, 100 *x* grid cells, and 100 *y* grid cells. I found the computational requirements for an exhaustive grid search quickly becomes prohibitive even for small search grids (≤ 200 X 200 cells). The optimization approach implemented to the backazimuth method was gradient descent, which is a classical means in mathematics for solving nonlinear problems (Ge, 2003).To implement gradient decent I consider an objective function

$$f(x_i, y_i) = \left\| \sum_{j=1}^{N_w} (\theta_i^m - \theta_i^c)^2 \right\|. \quad (8)$$

Here θ_i is a symmetric matrix of all angle differences between each combination of events corresponding to the measured (θ_i^m) and calculated (θ_i^c) differences, and the square is an elementwise operation. Index *i* represents each event and index *j* is the counter for the observation wells. For the case of a given monitor well and three events the matrix would appear as

$$\begin{bmatrix} 0 & (\theta_2^m - \theta_1^c)^2 & (\theta_3^m - \theta_1^c)^2 \\ (\theta_1^m - \theta_2^c)^2 & 0 & (\theta_3^m - \theta_2^c)^2 \\ (\theta_1^m - \theta_3^c)^2 & (\theta_2^m - \theta_3^c)^2 & 0 \end{bmatrix}$$

Gradient descent exploits the objective function's first derivative to find the minimum of the function. The minimum would correspond to the lowest error between calculated and measured azimuth angle differences. Gradient descent works extremely

well when the objective function is simple, lacking multiple minima or valleys. If not, these local minima can prevent the search from converging to the correct location (global minimum).

The first step to applying gradient descent to the code was to set up a trial model. I define the *x, y* locations of the three monitor wells to have an optimum spatial arrangement that minimizes the input error from spatial geometry. Next, I enter the true azimuths for the events, which generate the θ_i^m necessary for the objective function. Gradient descent is designed to find the minimum of the function, where the gradient of the function is exploited to find the minimum point. When this point is reached, the error between θ_i^m and θ_i^c (Equation 8) is the lowest and the corresponding *x, y* locations of the microseismic events are plotted.

Perf Shot Data Application

Real monitor array geometry was applied to the back azimuth technique. The real data were acquired near Allison, Texas where the Granite Wash Formation was targeted. It is not an ideal geometry and monitor well spacing is poor, but the array is typical of what may be encountered with real data. Perforation shots were recorded by the downhole array of geophones at each monitor well. During well completion 23 perforation shots were recorded over nine stages, and the measured depths along with the well deviation survey provided the absolute location of these shots. The model assumes that the deviation survey had no error in its azimuth information. Multiple perforation shots were fired during each stage; shot locations were averaged for each stage, and my models use the average locations as the absolute locations.

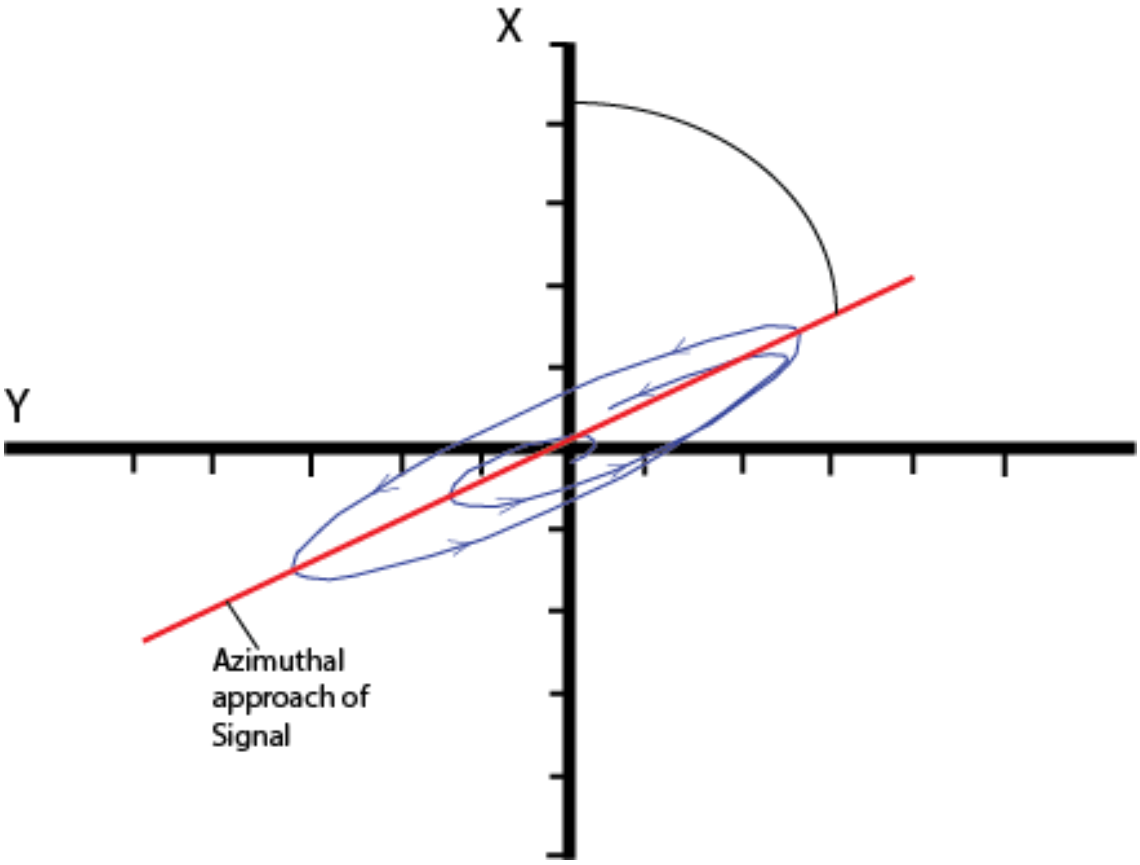

Figure 7. Schematic hodogram of particle motion in the *x, y* plane; detected by a three component geophone (after Ge, 2003).

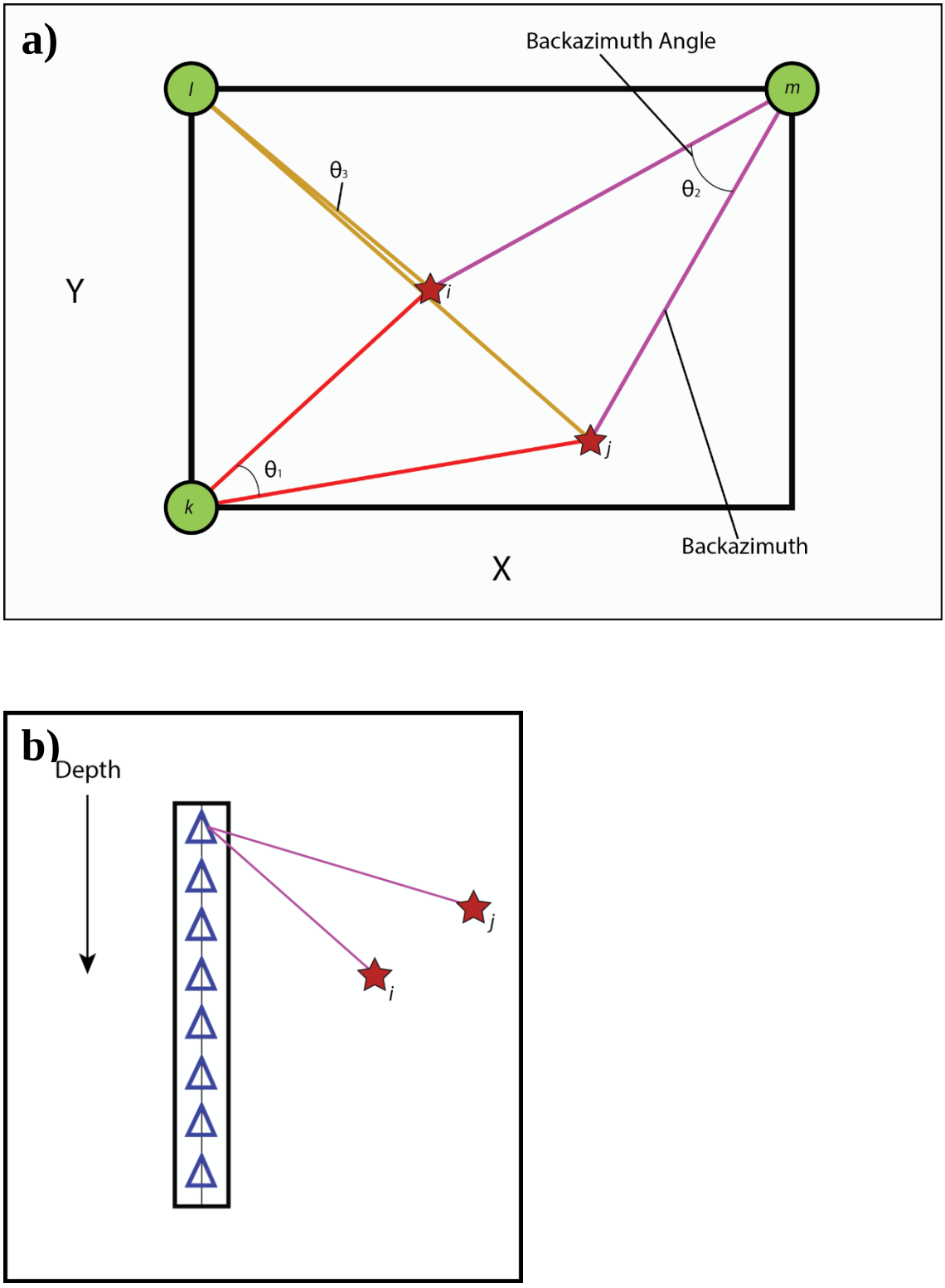

Figure 8. (a) Schematic of the back azimuth location method. Event are located without any velocity model information. (b) Schematic cross section showing two events used for the back azimuth analysis.

Chapter 4: Results

The results will show the test outcomes for the objective function in grid search, the simultaneous location of multiple events in gradient descent, and the application of a realistic, non-ideal monitor array geometry to the differential backazimuth angle method.

Grid Search

As mentioned earlier, the objective function I seek to minimize is controlled by the residual between $\Delta\theta_i^m$ and $\Delta\theta_i^c$. Where $\Delta\theta_i^m$ is the measured differential backazimuth angle and $\Delta\theta_i^c$ is the calculated, or predicted, differential backazimuth angle. These angles are derived from multiple microseismic events at a common monitor well in the horizontal plane. Thus, the residual between the different backazimuth angles is a function of four variables: x_1, x_2, y_1, and y_2. Using the grid search I have found it effective to hold two of these variables constant while I vary the other two for a contour plot of the resulting objective function. The correct location of the first event (x_1, y_1) is fixed in order to examine the error for all possible positions of the second event (x_2, y_2).

The grid search tests revealed that the grid sampling largely controls the error for calculated events and computation time drastically increases as the grid sampling is increased. For the search, a distribution of 100 X 100 cells was created to span the 1500 X 1500 ft area. With this arrangement, sampling nodes were 15 ft apart from one another. True event locations were placed at sampling nodes 15 ft from one another. With this narrow event spacing, the grid search correctly found the global minimum to

be at the true event location (Figures 9 and 10). However, when the true locations are slightly shifted to be ten ft from the nearest node the global minimum no longer aligns with the true location (Figures 11 and 12). As a follow up test, true locations were moved and separated by nearly 700 ft with one event being placed on a node and the second being 8 ft from the nearest sampled point. The global minimum for event 1 is nearly 100 ft from the absolute location (Figures 13 and 14). In further tests, absolute locations were placed with wide and narrow spacing near the area boundaries while still falling on nodes. In both instances the global minimum accurately aligns with the absolute location (Figures 15 – 18). In Figures 19 and 20 I show the plots of an event being placed at a node while the second event is completely off the grid. As a result, the global minimum is nearly 200 ft from the true location.

Computation time for a cell distribution of 100 X 100 within the 1500 X 1500 ft parameter space utilizing three monitor wells and two events was nearly 20 minutes using a single processor. To create a finer sampling grid, the cell distribution was changed to 200 X 200. The resulting node spacing was 7.5 ft. However, computation time for this finer grid jumped from 20 minutes to nearly 9 hours using the same computer system. A possible solution to lower the grid search computation time is to parallelize the program's coding. Parallelization would divide the grid search into steps, which could be solved simultaneously by multiple processors. This process would greatly reduce the computation time involved when running the grid search.

Gradient Descent

Gradient descent served as a method to simultaneously locate more than two events. In small grids the initial guess is trivial and correct convergence will be obtained

from any starting point (Figures 21 and 22). Generally, when the initial guesses are close to the true location, the algorithm requires fewer iterations to reach the convergence threshold.

Perf Shot Data Application

A realistic monitor array geometry acquired near Allison, Texas was applied to the differential backazimuth angles method. Events can be located with accuracy contingent upon the initial event guesses being +/- 50 ft from the true location (Figures 23 and 24). Close initial guesses cause the objective function to start small, thus ensuring that convergence is reached. Results indicate that the backazimuth location approach will correctly locate microseismic events, and six or more events are required to obtain convergence when the search's initial guesses are randomized. However, with initial guesses close to the true locations correct convergence requires as few as three events.

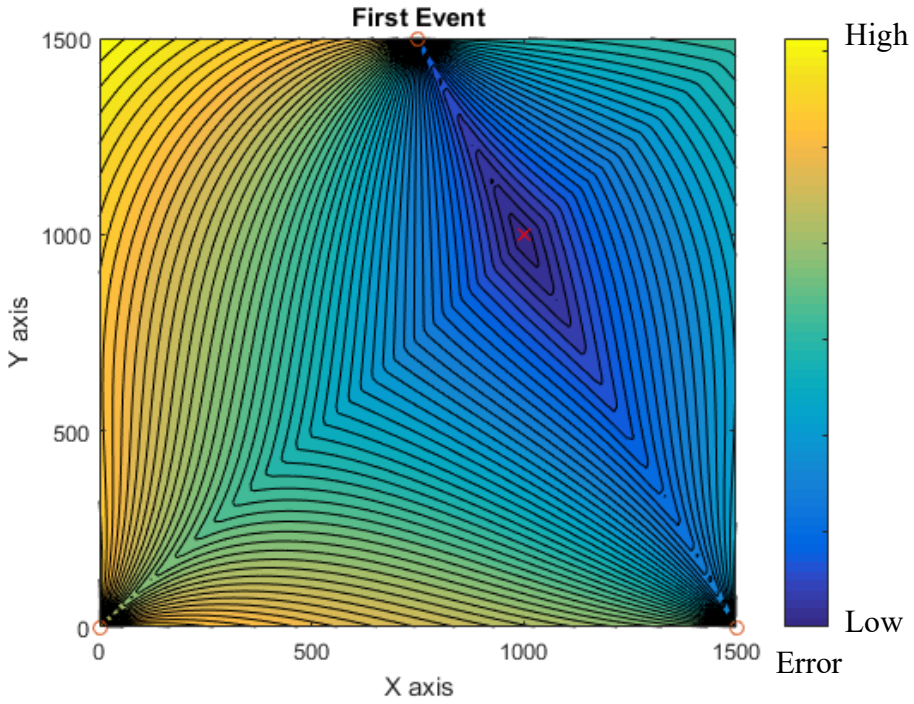

Figure 9. Contoured objective function (units in ft) where event 1 is fixed and its absolute location shown (red X).

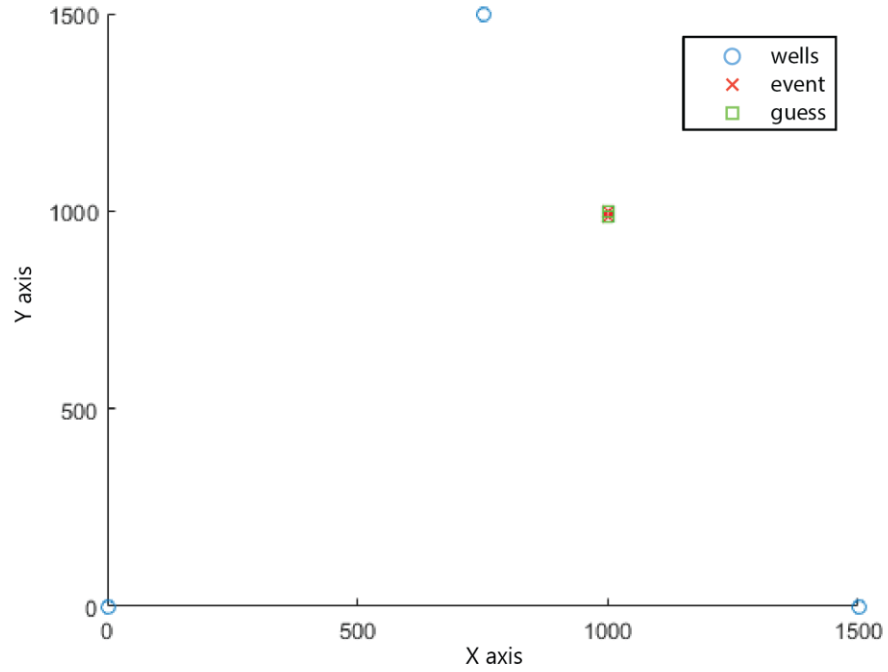

Figure 10. Scatter plot of the absolute locations of the two events and the calculated guesses. See contour plot above.

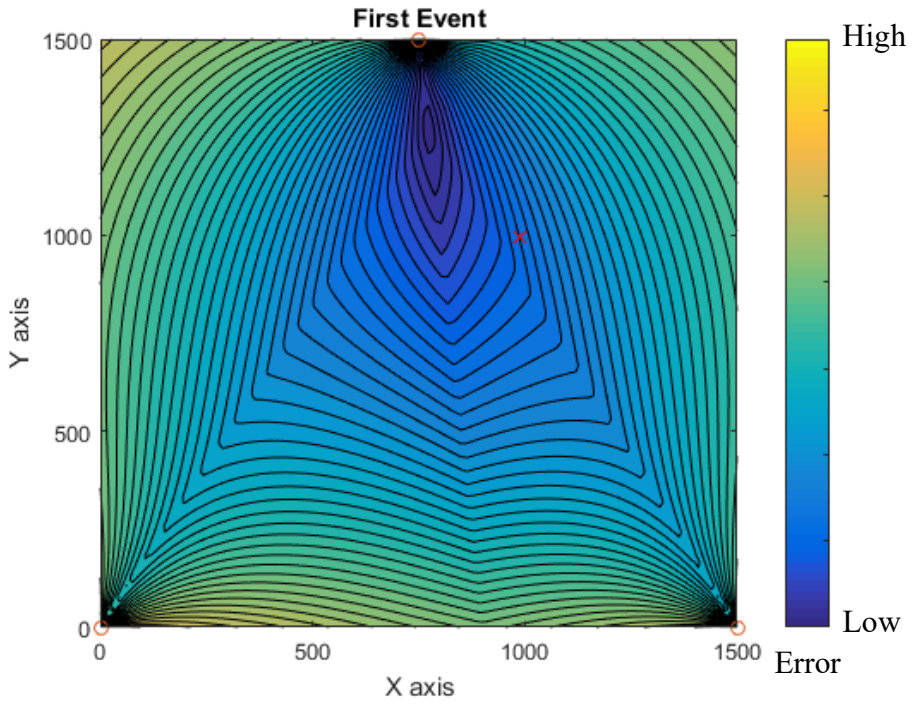

Figure 11. Contoured objective function (units in ft) where event 1 is fixed and its absolute location shown (red X). Events are nearly 15 ft apart from one another, but both events are off from sampled nodes.

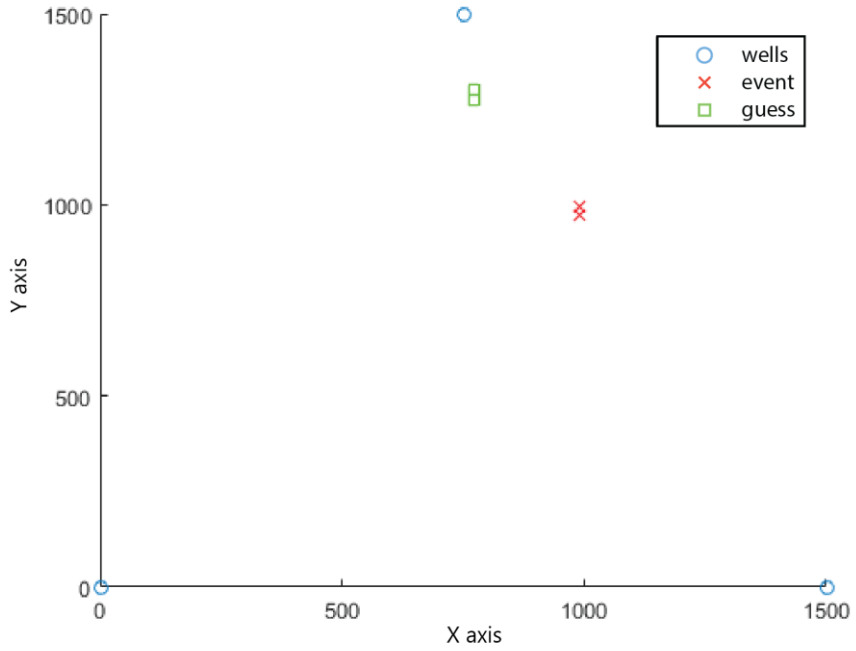

Figure 12. Scatter plot of the absolute locations of the two events and the calculated guesses. See contour plot above.

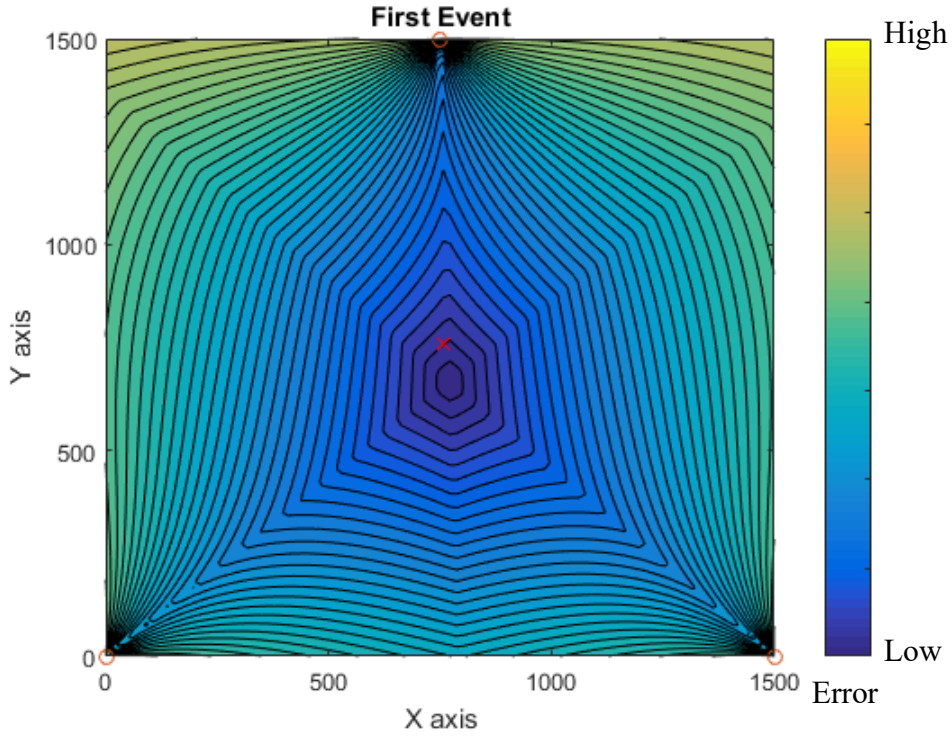

Figure 13. Contoured objective function (units in ft) where event 1 is fixed and its absolute location shown (red X). Events are nearly 700 ft apart from one another with only event one being located on a node.

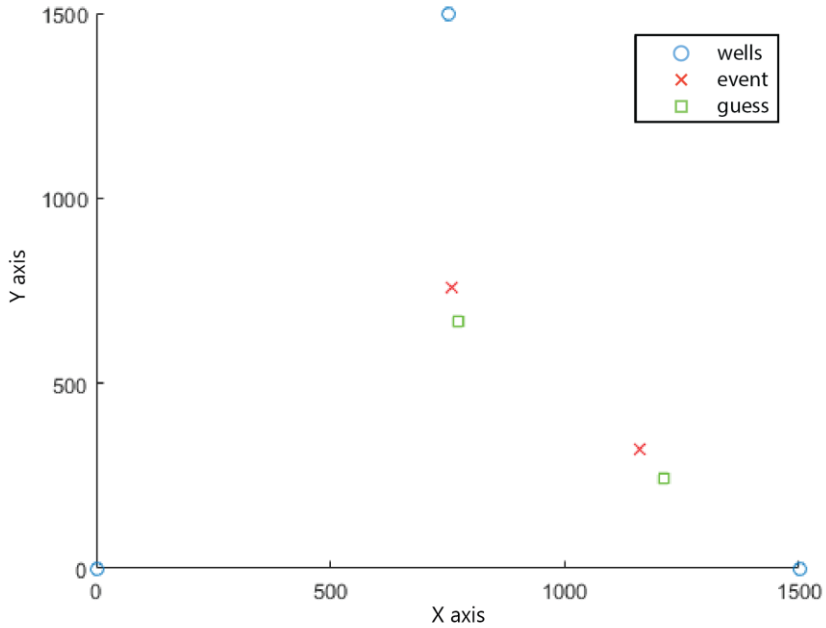

Figure 14. Scatter plot of the absolute locations of the two events and the calculated guesses. See contour plot above.

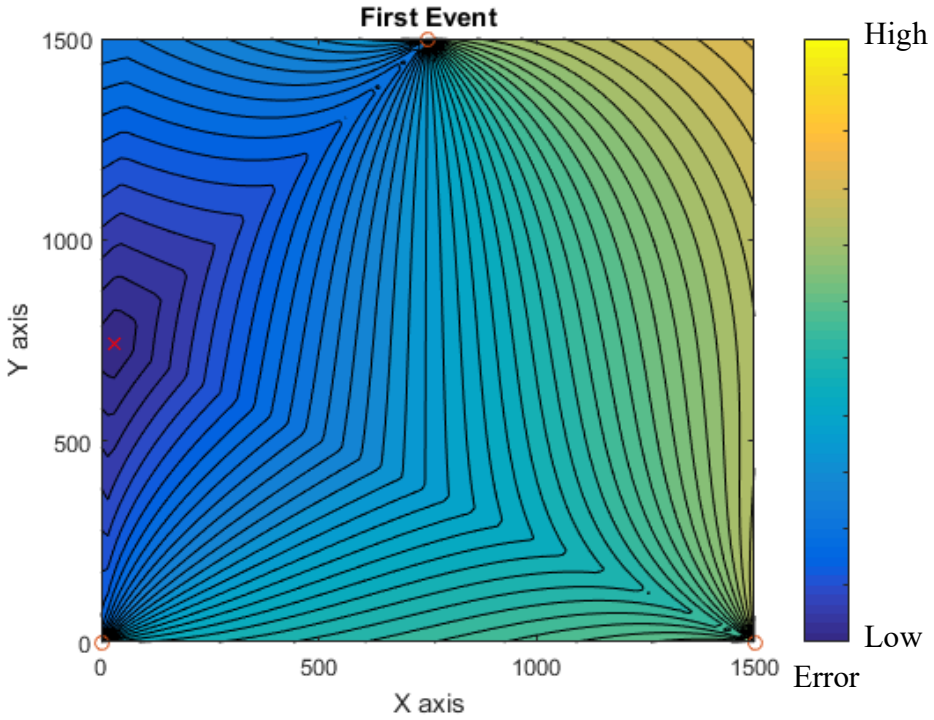

Figure 15. Contoured objective function (units in ft) where event 1 is fixed and its absolute location shown (red X). Events are nearly 1500 ft apart from one another; both events are located on nodes.

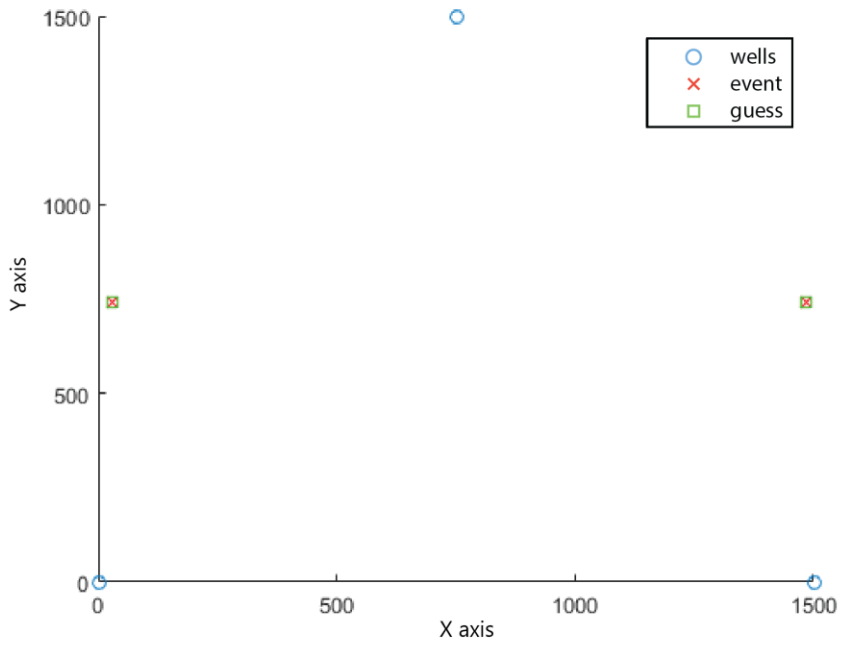

Figure 16. Scatter plot of the absolute locations of the two events and the calculated guesses. See contour plot above.

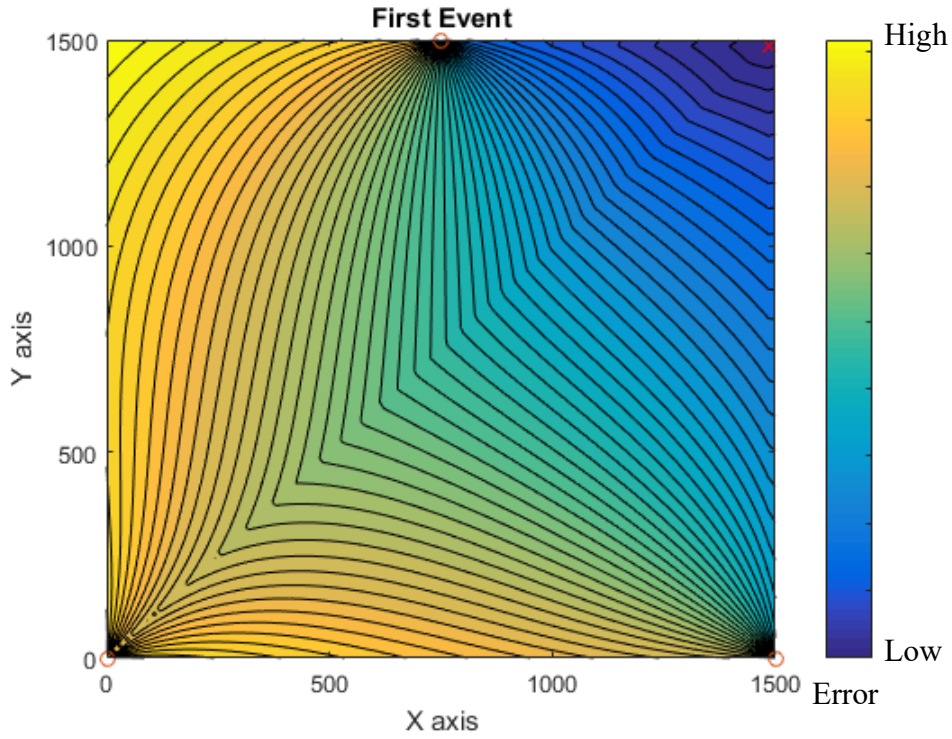

Figure 17. Contoured objective function (units in ft) where event 1 is fixed and its absolute location shown (red X). Events are nearly 15 ft apart from one another and located on nodes near the grid boundary.

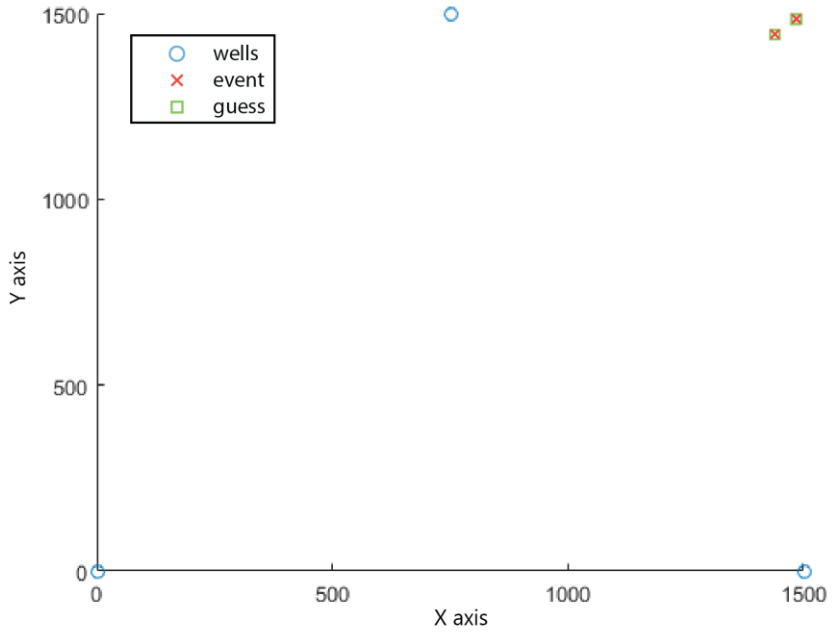

Figure 18. Scatter plot of the absolute locations of the two events and the calculated guesses. See contour plot above.

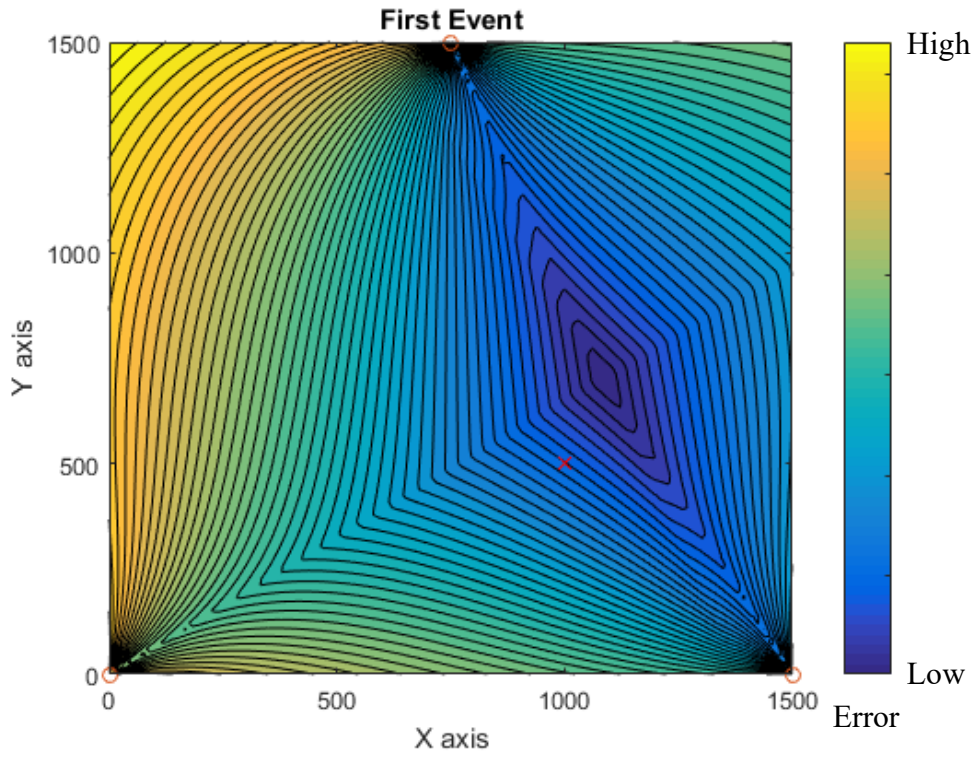

Figure 19. Contoured objective function (units in ft) where event 1 is fixed and its absolute location shown (red X). Absolute location of event one is on a node while the second event's absolute location is off the grid.

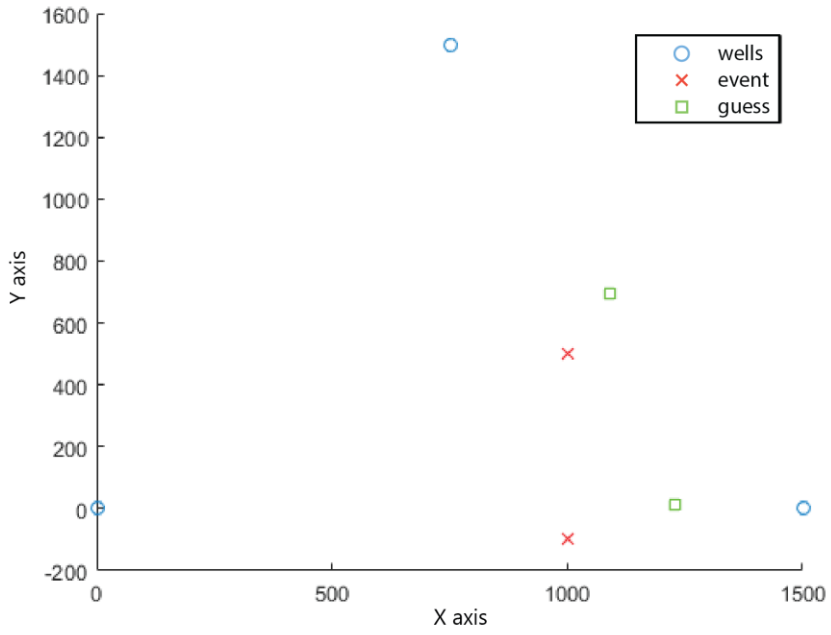

Figure 20. Scatter plot of the absolute locations of the two events and the calculated guesses. See contour plot above.

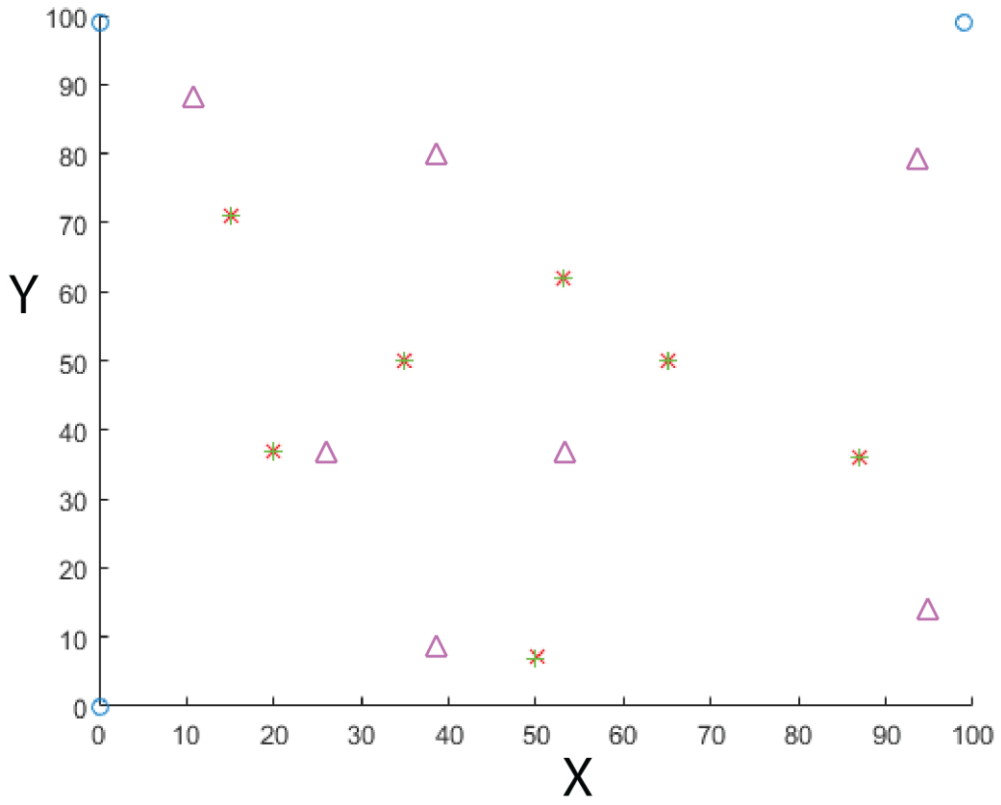

Figure 21. Gradient descent models reveal that microseismic source location can be determined using only azimuth information. Red x's are the known locations, green +'s are the calculated locations, purple Δ's are initial guess solutions, and blue o's are monitor wells.

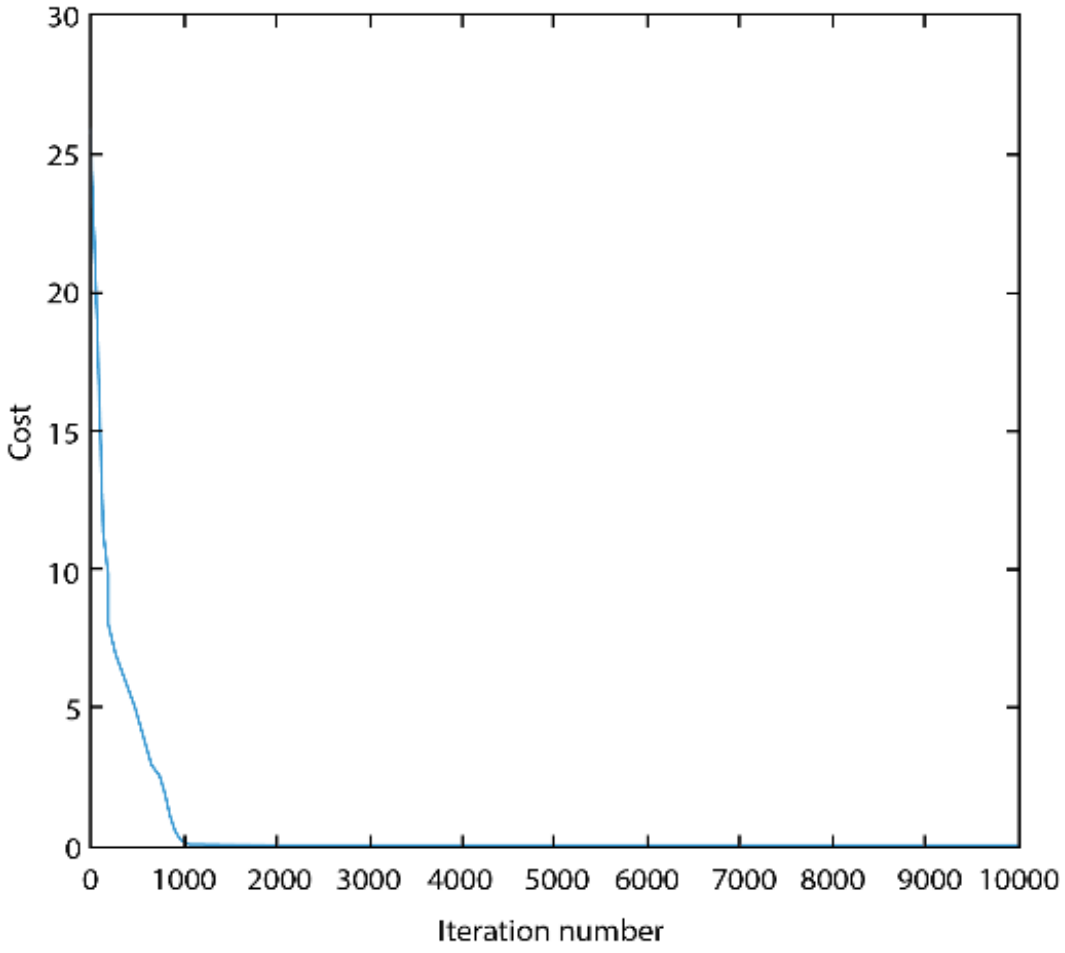

Figure 22. Cost function for gradient descent location shown in Figure 21. Algorithm convergence is generally obtained within 2000 iterations.

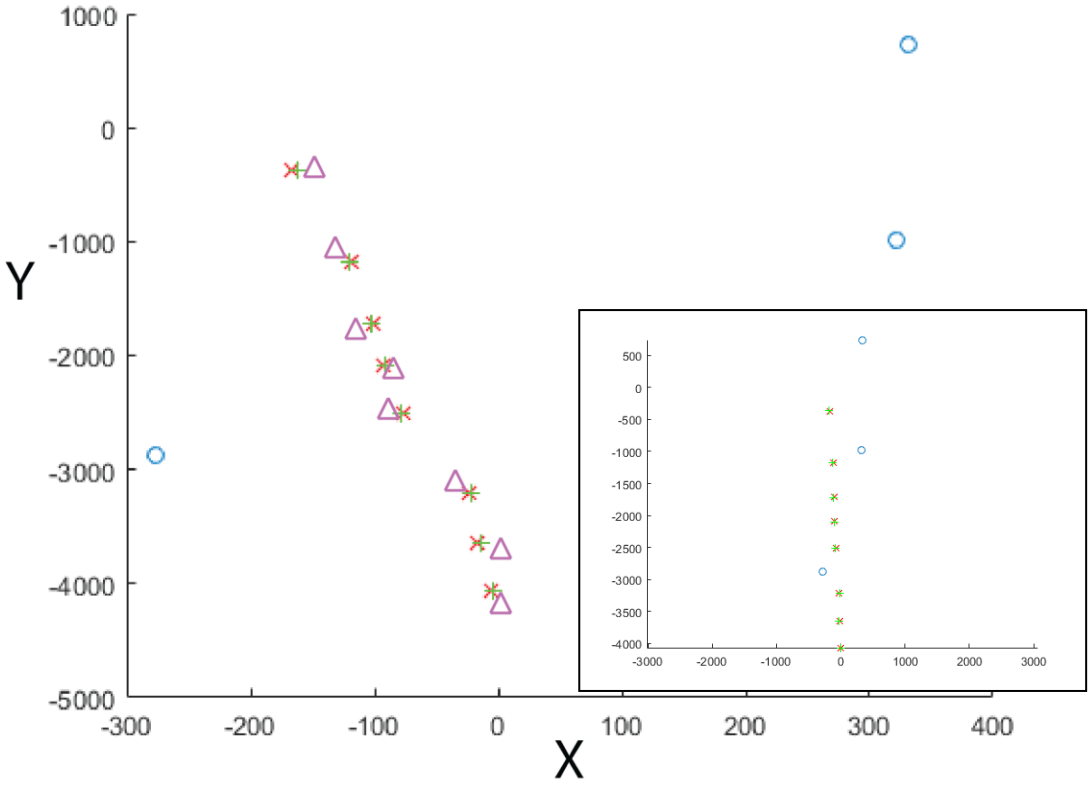

Figure 23. Gradient descent search algorithm applied to a realistic monitor array geometry. Inset map displays monitor array geometry with the *x, y* axes having the same scale. When the algorithm's initial guess is close to the absolute location the differential backazimuth method provides accurate locations. Red x's are the known locations, green +'s are the calculated locations, purple Δ's are initial guess solutions, and blue o's are monitor wells.

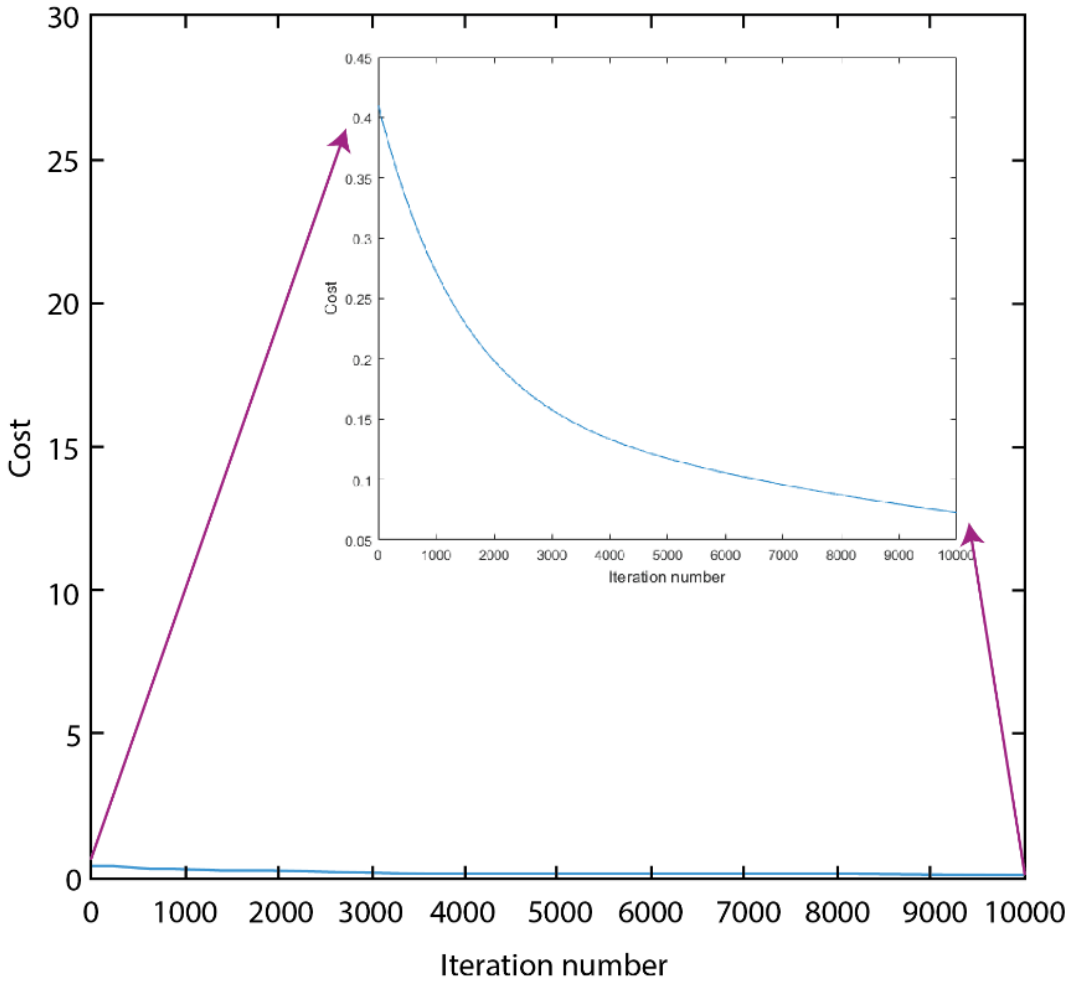

Figure 24. Cost function of the gradient descent applied to a realistic monitor well array geometry (see Figure 23). Real array geometry requires an initial guess that has a small objective function. Plot is magnified to verify function's convergence.

Chapter 5: Discussion

Results from the grid search method confirm the feasibility of locating a combination of microseismic events using only differential backazimuth angle information and no velocity model, where a minimum of three monitor wells are used to record relative azimuths to the events. The search also reveals the limits of the grid sampling and extensive computation time. In gradient descent the results indicate more than two events can be located simultaneously in a fraction of the computation time required by grid search. The design of the algorithm allows for events to be located even when geophones are randomly oriented. Thus, the approach is beneficial when calibration shots are unavailable, difficult to obtain, or contain significant error. Application of real monitor array geometry showed that the differential backazimuth method will locate events even when the search area is large (approximately 5000 X 1000 ft), but poor monitor array geometry necessitates the initial guess being within 50 ft of the true location.

Grid Search

From the grid search method I learned that microseismic events could be located in the horizontal plane with only azimuthal information. The search performs best when the sampling points, or nodes, are close to the minimum error location. If this is not the case, the search would under sample the objective function and calculate events with larger error. In an effort to correctly sample the objective function, I edited the grid to be 200 X 200 cells where cell nodes where 7.5 ft apart from each other. Even with such sampling the calculated locations persisted with error unless true locations were placed

at sampling points. I expect that as node spacing decreases the oversimplification will be eliminated and events will be correctly calculated, however such fine sampling would greatly elevate the computation time for the search. Grid search will locate events using only differential backazimuth angle information, however a fine sampling space is required to ensure accurate location of calculated events.

As referred to earlier, a concern with grid search is the computation time owing to search evaluating every node location. All possible backazimuth angle differences are calculated at each node, and these calculated angles are compared to the observed angle. The search's sampling may entirely miss where the true minimum is located (Figure 25). This under sampling diminishes grid search's ability to accurately locate events, but when the grid is edited to have finer sampling the computation time drastically increases. These observations of the tradeoff between sampling and computation time make application of the search to a real array difficult. Results from the grid search partially aligned with the expectations that events would be accurately located, since every cell within the area is evaluated in the search process. It was originally thought that the relative and absolute spacing of events would influence the error between the global minimum and the true location. Instead, I found absolute and relative spacing had no effect on the search. Location error was caused by under sampling of the parameter space.

When compared to the abilities of Geiger's Method and the Double-Difference Method, the grid search performs well in small areas, but the inadequacies in sampling and computation time cause the method to be limited in its ability to locate events with

low error. This error could also be linked to the objective function being nonlinear, which creates local minimum that do not correspond to the true location.

Gradient Descent

Gradient descent proved to be an effective optimization algorithm that would locate more than two events simultaneously in a fraction of the time required by grid search. The inclusion of more than two events provided more differential backazimuth angles to constrain event locations and provide an objective function with a better separated global minimum. Increasing the number of events that can be located while dropping the computation time allowed for later application to real array geometries. Locating many microseismic events in a short amount of processing time makes gradient descent an ideal approach to be applied to real data. During hydraulic fracturing, hundreds of microseismic event are recorded by downhole arrays of randomly oriented geophones and their backazimuths are derived from the resulting hodograms. By exploiting the differential backazimuths angles, I am able to determine the events' locations even with randomly oriented geophones.

In the synthetic models one assumes lateral homogeneity and no horizontal ray bending; thus the backazimuth method is able to provide an absolute location for microseismic events in the *x, y* plane completely independent of the velocity model. Velocity models will only account for velocities within the monitor array coverage, and any anomalies outside of the coverage area would be ignored (Figures 26 and 27). When these missed anomalies come between a monitor well and an event, the event will be completely mislocated with traditional techniques such as Geiger's Method. Under

the assumptions stated earlier, the differential backazimuth angles would not be influenced by the anomaly and would still provide an *x, y* location for the event.

In comparison to the grid search, the gradient descent search is a fraction of the computation time. The grid search located two events within a 2,250,000 square foot area in nearly 20 minutes, while gradient descent searched within an area twice as large and located seven events in approximately three minutes. Decrease in processing time is due to the algorithm exploiting the function's gradient in place of evaluating every cell node within the area. In order for the algorithm to correctly converge using the function's gradient, it is imperative the monitor array and event geometry be designed such that the wells be ideally spaced. Proper array geometry would help ensure the search algorithm will correctly locate the global minimum. In relation to real events recorded during a stage of hydraulic fracturing, initial guess locations would be drawn from the results of a traditional method; anisotropy and preexisting fault systems would also need to be considered when making an initial guess for possible microseismic events.

A key benefit from the backazimuth method is its ability to locate microseismic events when borehole geophones are randomly oriented or contain orientation error. In traditional methods, geophones are oriented by using calibration shots, or perf shots, which allow for the geophones' orientation to be corrected. However, the known locations of perforation shots are not always accurate. The deviation survey provided by drillers can have large errors that will label erroneous locations as the true locations for perf shots (Bulant et al., 2007) (Figure 28). Such error will cause backazimuth angles to be misinterpreted and event locations to be calculated with large error. The differential

backazimuth method remedies this problem by not requiring oriented geophones, which in turn eliminates the need for calibration shots.

Perf Shot Data Application

Application of the search algorithm to real array geometry proved that events can be located when the search area is large and monitor array geometry not ideal. For the gradient descent synthetics shown earlier, the area size was 100 X 100 ft, but the real array geometry has dimensions of nearly 5000 X 1000 ft. These dimensions are typical for wells being hydraulically stimulated within the Granite Wash Formation. The three monitor wells are not spaced ideally for microseismic monitoring: wells have uneven spacing and do not encompass all of the perforation shots. This is common for observation wells, since many are wells that were not drilled with the intent to monitor microseismic events. Their proximity to a treatment well qualifies them as monitor wells, but their spatial arrangement is usually non-ideal. In Figure 23 the perforation shot locations are accurately calculated with the differential backazimuth method. However, the initial guess is still critical for gradient descent to correctly converge owing to the poor array geometry. Results show that initial guesses for events must be within 50 ft of the true location to have a correctly calculated event location. With this criterion met, the nonlinear objective function can be navigated with gradient descent and multiple microseismic events can be properly located.

A modified workflow of traditional methods can be used to locate microseismic events and improve events' locations when the velocity model is poor (Figure 29). For such instances, Geiger's Method could be used to locate events but error from the poor velocity model would persist in the events' *x*, *y* locations creating a large microseismic

cloud (Figure 30). To improve this location, the differential backazimuth method could first be conducted to locate microseismic events in the horizontal plane. Thus, error from a poor velocity model would not affect events' locations. These initial locations, provided by the differential backazimuth method, can be used to constrain and improve the velocity model after which the traditional method would be reapplied. It is expected that with an improved velocity model the microseismic clouds shown in Figure 30 would collapse to image the fracture pattern of the stage (Figure 31). This expected result would be similar to results seen in the Double-Difference method where widely distributed events have been relocated to image narrow regions along fault zones. Implementation of the differential backazimuth approach to a traditional method can provide better microseismic locations when velocity models are poor.

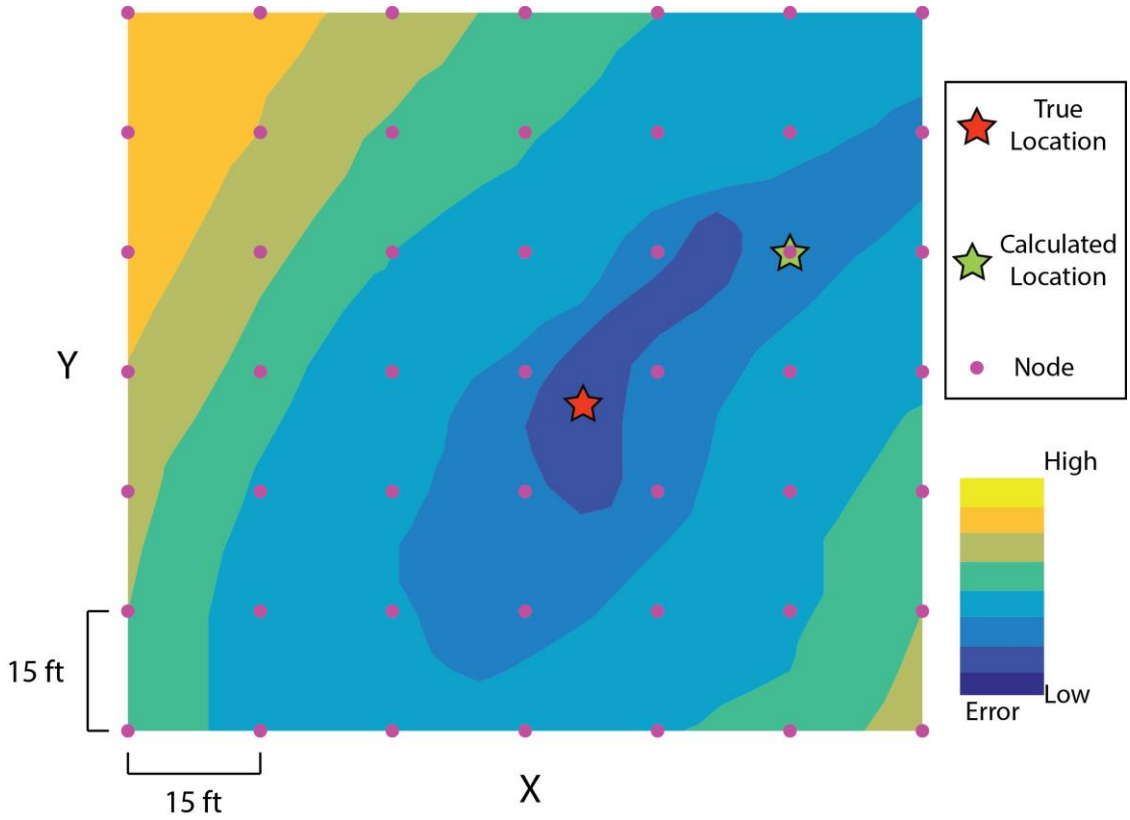

Figure 25. Schematic of the sampling of grid search in order to find the minimum of the contoured objective function. The sampling error of grid search may be under sampling the objective function and causing error in the calculated locations.

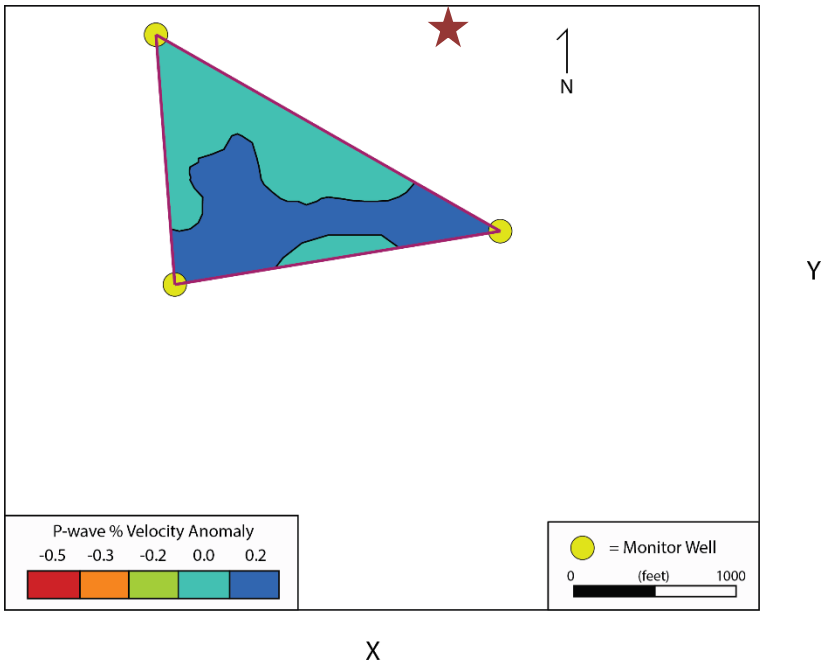

Figure 26. The contoured velocity model anomalies taken from velocity information at the three monitor wells. Brown star indicates a microseismic event located outside the array using the wells' velocity model.

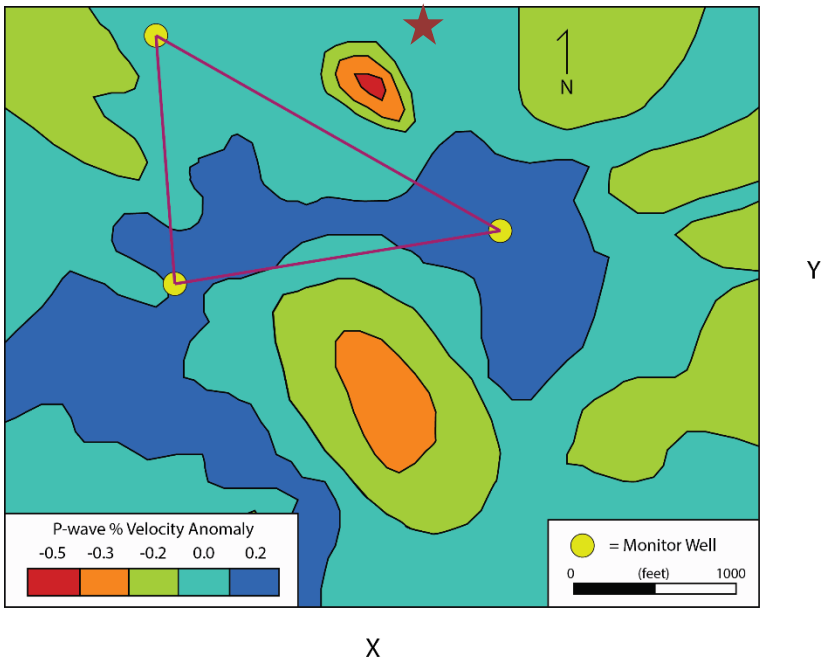

Figure 27. The actual velocity model anomalies for the area. The velocity model in Figure 26 would not image the northern anomaly and using the velocity model for the northern event (red star) would result in high location error.

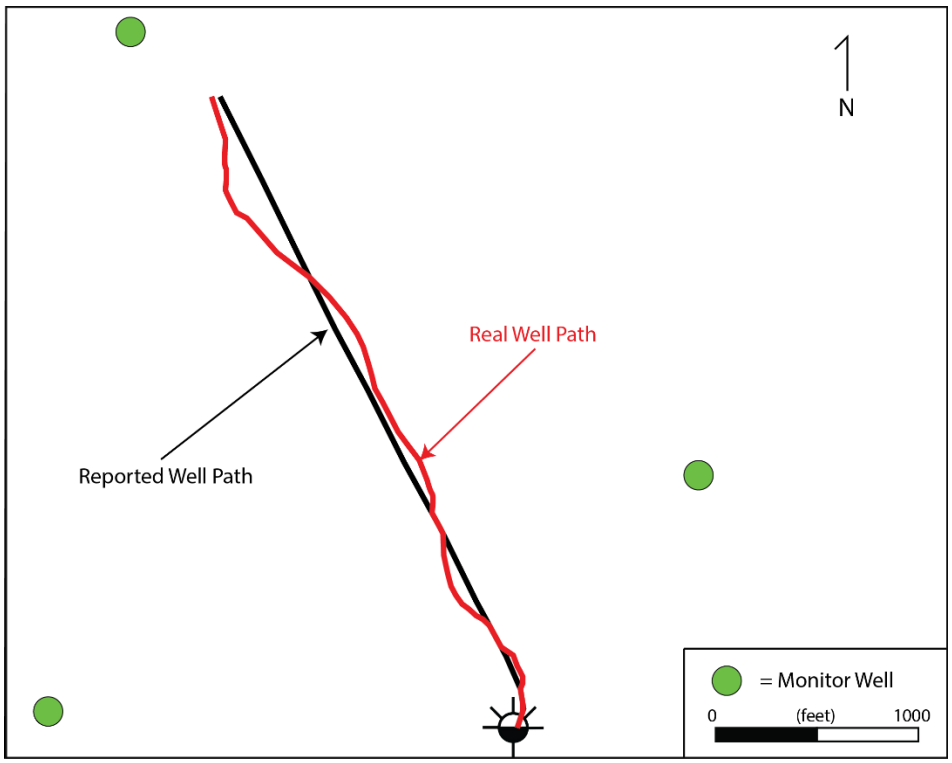

Figure 28. Schematic of the reported well path and the actual well path. Calibration shot locations based on reported well paths often have location errors that will affect geophones when an orientation correction is applied.

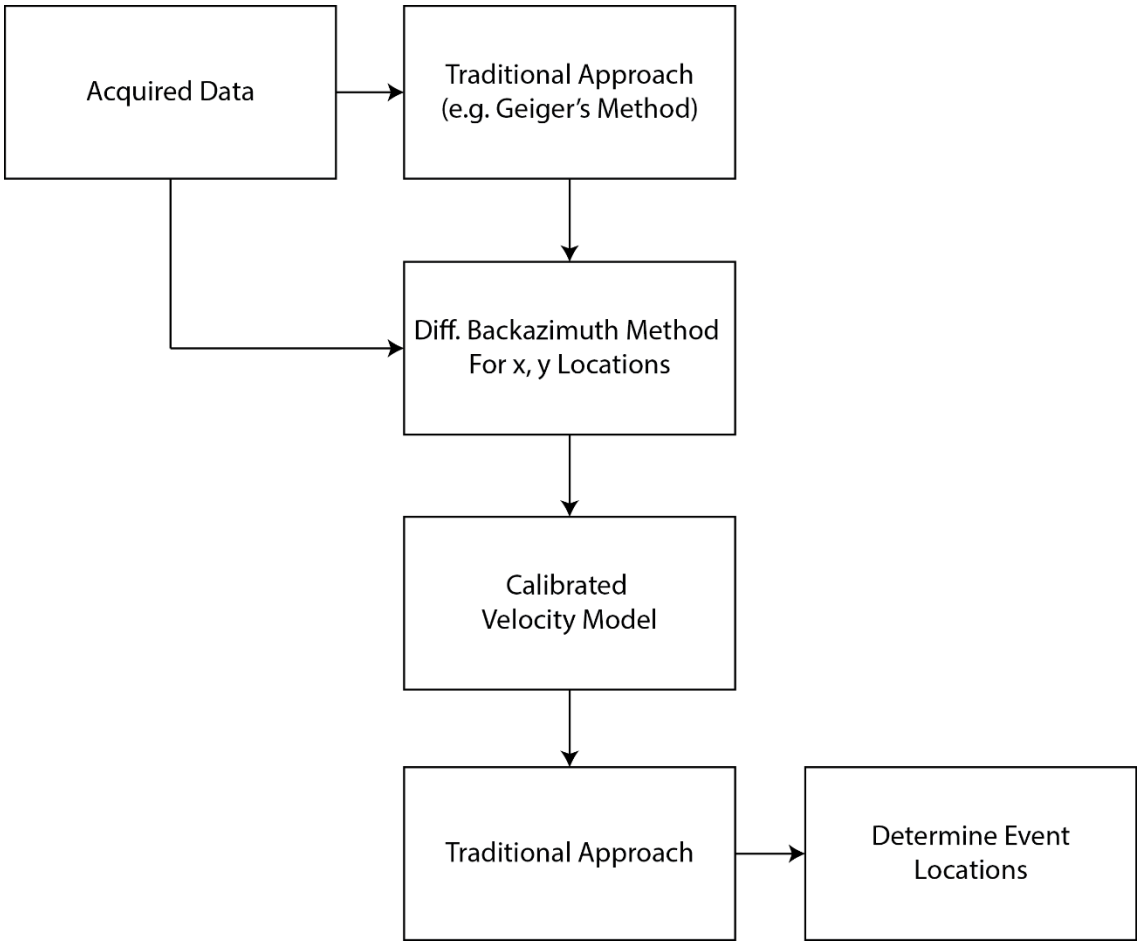

Figure 29. Modified location workflow that incorporates the differential backazimuth method in either the first or second step for a calibrated velocity model.

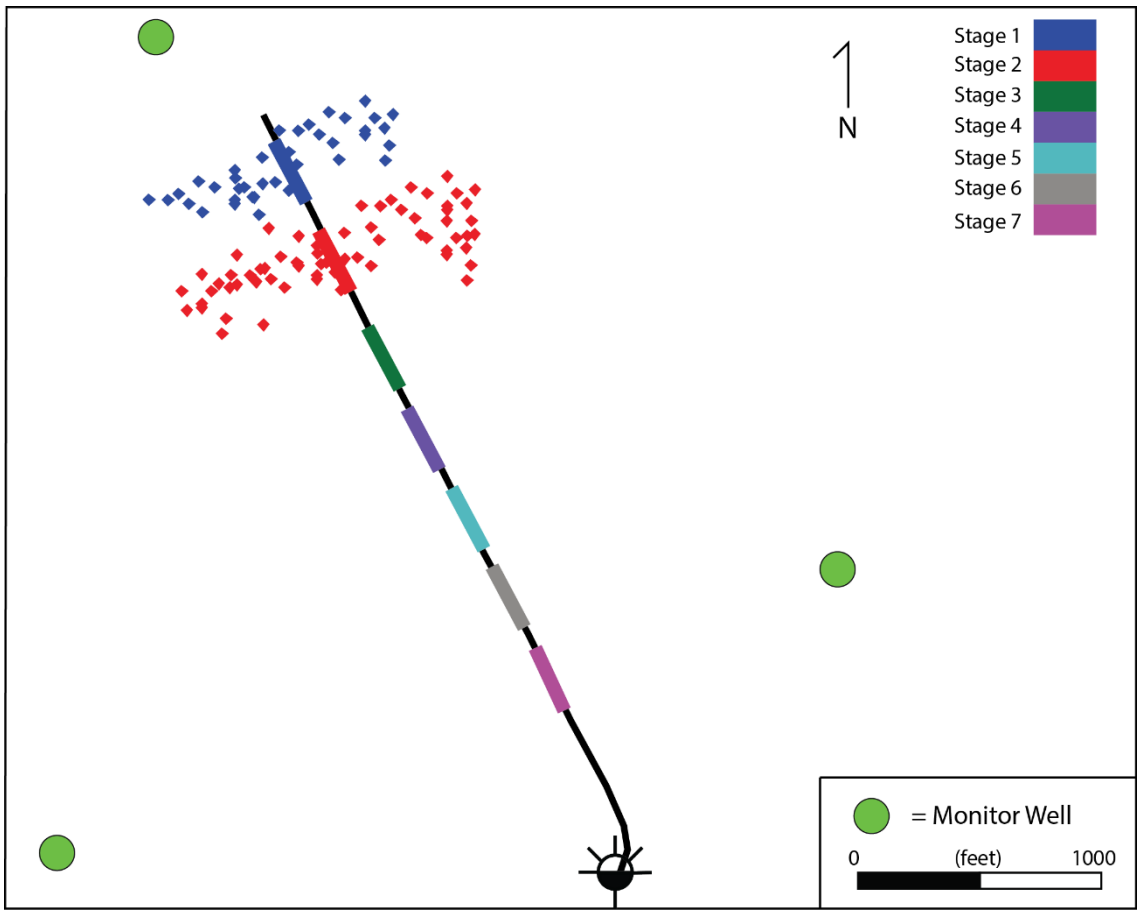

Figure 30. Schematic of two stages of microseismic events that have been located using the traditional approach with a poor velocity model. Notice the wide spacing of events in microseismic clouds.

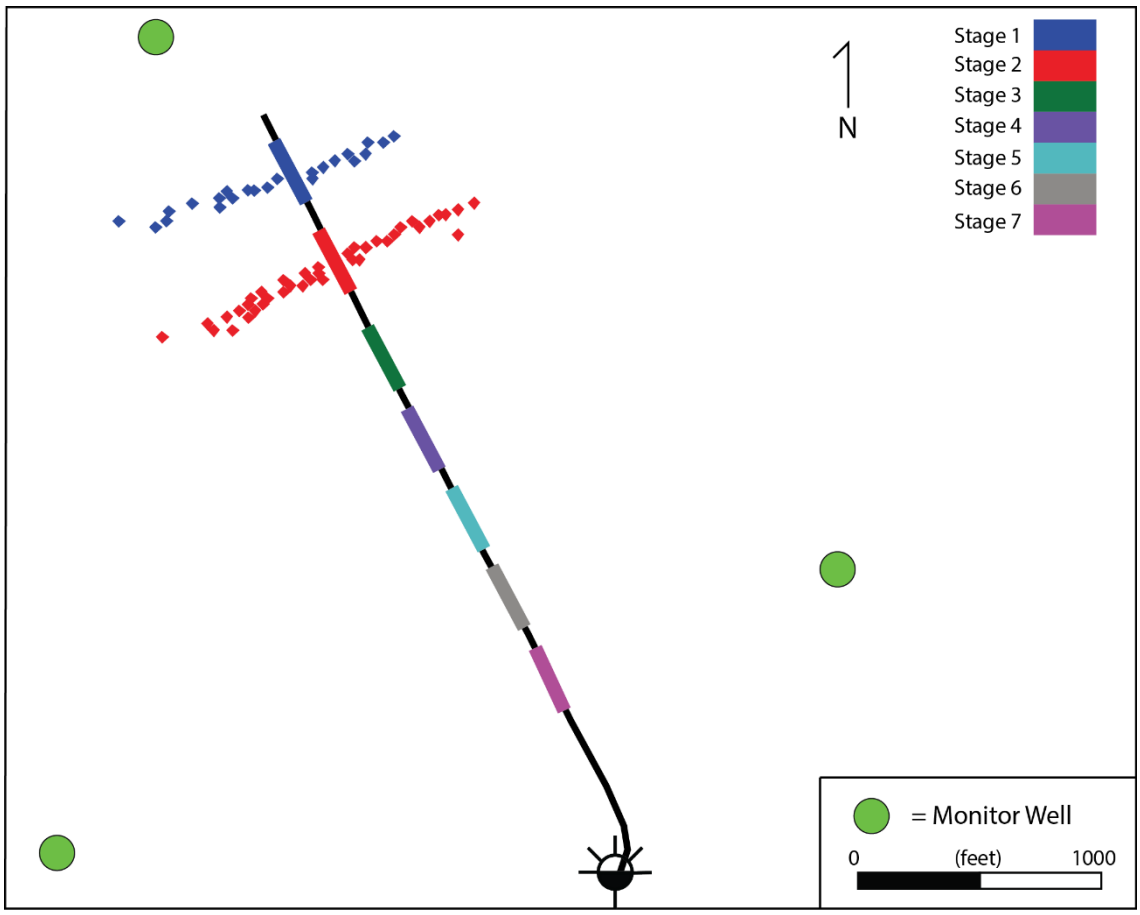

Figure 31. Schematic of two stages of microseismic events that have been located using the modified location approach that incorporates the backazimuth method. The backazimuth method would allow for better calibration of the velocity model. Microseismic clouds would collapse to better image fractures resulting from hydraulic stimulation.

Chapter 6: Conclusions

Common procedures for locating microseismic events rely on differences in arrival time and oriented geophones. I have shown that events can be located using only differential backazimuth angles. The use of the differential backazimuth approach allows for events to be located without velocity model information or geophone orientation. To find events using the backazimuth method two search techniques are implemented: grid search and gradient descent. Grid search is a deterministic approach of dividing the search area into a uniform array of cells and analyzing each cell's differential backazimuth angles. Gradient descent exploits the objective function's derivative to calculate event locations associated with the smallest error between observed and calculated differential backazimuth angles.

Results from the grid search approach prove the feasibility of locating microseismic events in the horizontal plane using only differential backazimuth angle information. The contoured objective function from grid search reveals its complex nature and the presence of a global minimum. Even with a poor monitor array geometry, the gradient descent method will converge to the correct location when its initial guess is within 50 ft of the true location. With non-ideal, realistic monitor array geometries, gradient descent correctly locates events in the horizontal plane.

In the case where multiple monitor wells are available, it is possible to exploit backazimuth differences between events which eliminates the need for geophone orientation. The differential backazimuth method also facilitates initial location of events in the horizontal plane without the need for a velocity model. Initial horizontal

locations, provided by this new method, can be used to calibrate and improve the velocity model in the area for subsequent event location. This approach is beneficial when calibration shots are unavailable, difficult to obtain, or contain significant error. Further research will implement real events to the method, where the observed differential backazimuth angle will be derived from the hodogram. Owing to the objective function's complexity and the presence of local minima, other optimization approaches such as genetic algorithms or simulated annealing could be applied to ensure that the global minimum is always the calculated location.

References

British Geological Survey, 2016, How we measure earthquakes, http://www.bgs.ac.uk/discoveringGeology/hazards/earthquakes/HowWeMeasureThem.html, accessed April 19, 2016.

Bulant, P., L. Eisner, I. Psencik, and J.L. Calvez, 2007, Importance of borehole deviation surveys for monitoring of hydraulic fracturing treatments: Geophysical Prospecting, **55**, 891-899.

Durrani, M.Z., K. Willson, J. Chen, B. Tapp, and J. Akram, 2014, Rational rock physics for improved velocity prediction and reservoir properties estimation for Granite Wash (tight sands) in Anadarko Basin, Texas: International Journal of Geophysics, **2014**, 1-15.

Gay, S., 2014, Some observations on the Amarillo/Wichita Mountains Thrust-Fold Belt and its extensions southeast into East Texas and northwest into New Mexico: Shale Shaker, 338-366.

Ge, M., 2003, Analysis of source location algorithms Part I: Overview and non-iterative methods: Journal of Acoustic Emission, **21**, 14-28.

Ge, M., 2003, Analysis of source location algorithms Part II: Iterative methods: Journal of Acoustic Emission, **21**, 29-51.

Geiger, L., 1912, Probability method for the determination of earthquake epicenters from arrival time only, Bulletin of St. Louis University, **8**, 56-71.

Lee, W., and D. Dodge, 2010, Reliable earthquake location using grid-search and simplex algorithm: Presented at the Tsunami Source Working Group Workshop, USGS.

Li, J., H. Zhang, W.L. Rodi, and M.N. Toksoz, 2013, Joint microseismic location and anisotropic tomography using differential arrival times and differential backazimuths: Geophysics Journal International, 1-15.

LoCricchio, E., 2012, Granite Wash play overview, Anadarko Basin: stratigraphic framework and controls on Pennsylvanian Granite Wash production, Anadarko Basin, Texas and Oklahoma: Presented at the 2012 Annual Convention, AAPG.

Long, S., 2014, Fracture height growth characterization from microseismic data in the Granite Wash: M.S. thesis, University of Oklahoma.

Maxwell, S.C., 2014, Microseismic imaging of hydraulic fracturing: improved engineering of unconventional shale reservoirs: Society of Exploration Geophysicists.

Maxwell, S. C., T.I. Urbancic, N. Steinsberger, and R. Zinno, 2002, Microseismic imaging of hydraulic fracture complexity in the Barnett Shale, Presented at the SPE Annual Technical Conference and Exhibition, SPE.

Mitchell, J., 2011, Horizontal drilling of deep Granite Wash reservoirs, Anadarko Basin, Oklahoma and Texas: Shale Shaker, **62**, 118-167.

Poliannikov, O.V., M. Prange, A.E. Malcolm, and H. Djikpesse, 2014, Joint location of microseismic events in the presence of velocity uncertainty: Geophysics, **79**, KS51-KS60.

Sambridge, M., and K. Mosegaard, 2002, Monte Carlo methods in geophysical inverse problems: Reviews of Geophysics, **40**, 1-25.

Slunga, R., S.T. Rognvaldsson, and R. Bodvarsson, 1995, Absolute and relative locations of similar events with application to microearthquakes in southern Iceland: Geophysics Journal International, **123**, 409-419.

Waldhauser, F., and W.L. Ellsworth, 2000, A double-difference earthquake location algorithm: method and application to the Northern Hayward Fault, California: Bulletin of the Seismological Society of America, **90**, 1353-1368.

Zimmer, U., 2011, Calculating stimulated reservoir volume (SRV) with consideration of uncertainties in microseismic-event locations: Presented at the Canadian Unconventional Resources Conference, SPE.